Indirect/astrophysical searches

Indirect Dark Matter Searches

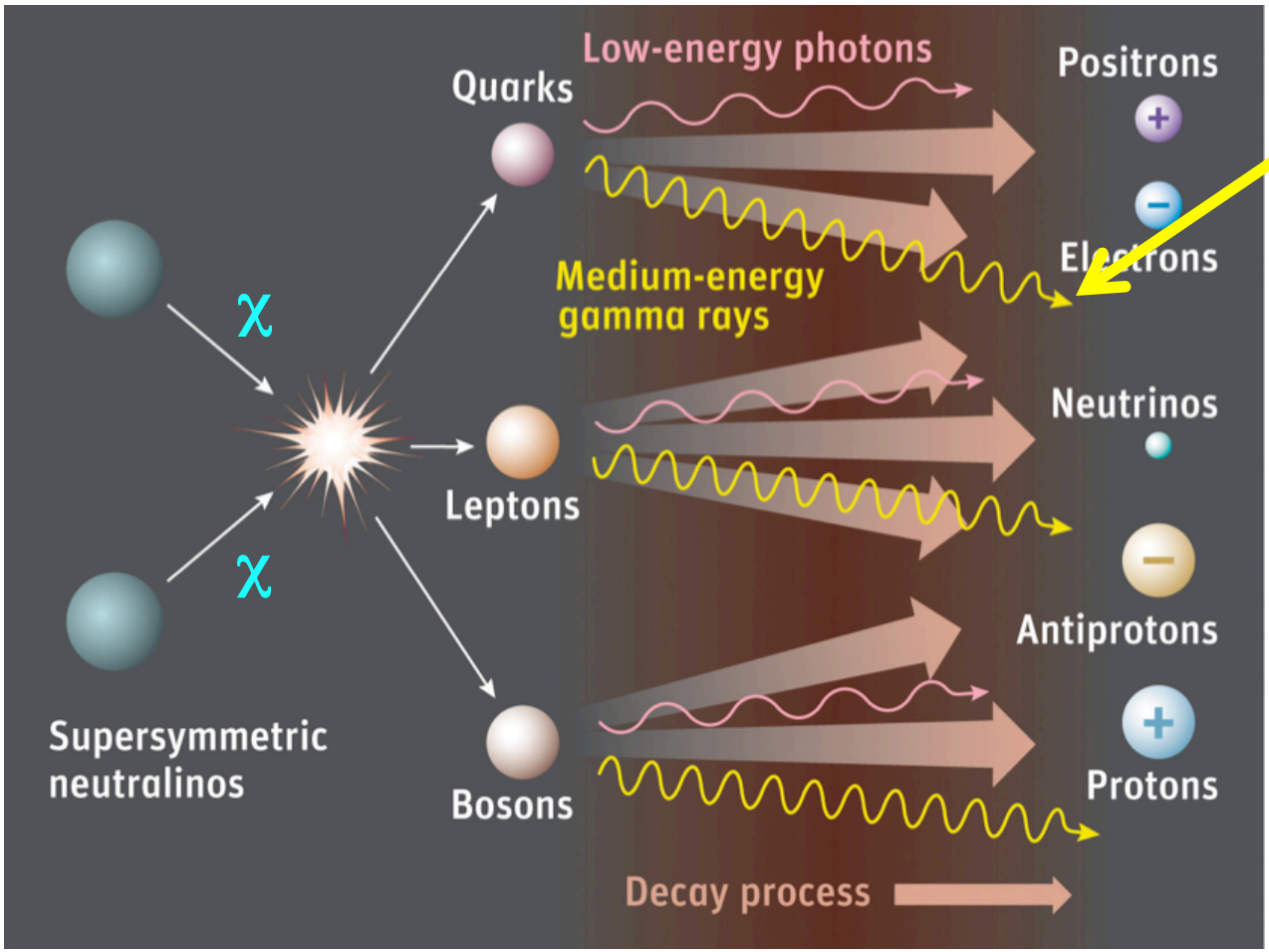

Detect gamma rays

Dark matter annihilation

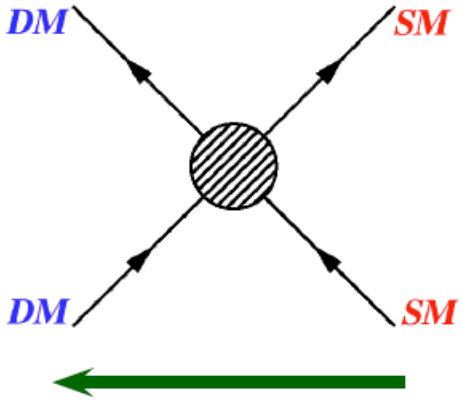

Production at colliders

Advantage: Neutral cosmic rays (gamma-rays) are not affected by interstellar & intergalactic magnetic fields (point back to source)
Complementary to indirect dark matter searches at colliders

Dark Matter Annihilation/Decay search

Expected gamma-ray flux:

$$\frac{d\Phi_\gamma}{dE} = \frac{d\Phi_\gamma^{PP}}{dE} J(\Omega)$$

Particle Physics factor:
photons per annhilation/decay

Astrophysical factor:
line-of-site integral of Dark Matter distribution

	Particle Physics factor	Astrophysical factor
Annihilation	$\frac{d\Phi_\gamma^{PP}}{dE} = \frac{\langle \sigma_{ann} v \rangle}{8\pi m_{DM}^2} \frac{dN_\gamma}{dE}$	$J(\Omega) = \int_\Omega \int_{los} \rho^2(r)\, dr\, d\Omega$
Decay	$\frac{d\Phi_\gamma^{PP}}{dE} = \frac{1}{4\pi m_{DM} \tau_{DM}} \frac{dN_\gamma}{dE}$	$J(\Omega) = \int_\Omega \int_{los} \rho(r)\, dr\, d\Omega$

Perform a likelihood fit on the measured gamma-ray flux

Produce 95% CL limits on:

- $\langle \sigma_{ann} v \rangle$: thermally averaged annihilation cross section
- τ_{DM} : DM particle decay life-time

as a function of the dark matter particle mass m_{DM}

Dark Matter: Astrophysical Sources

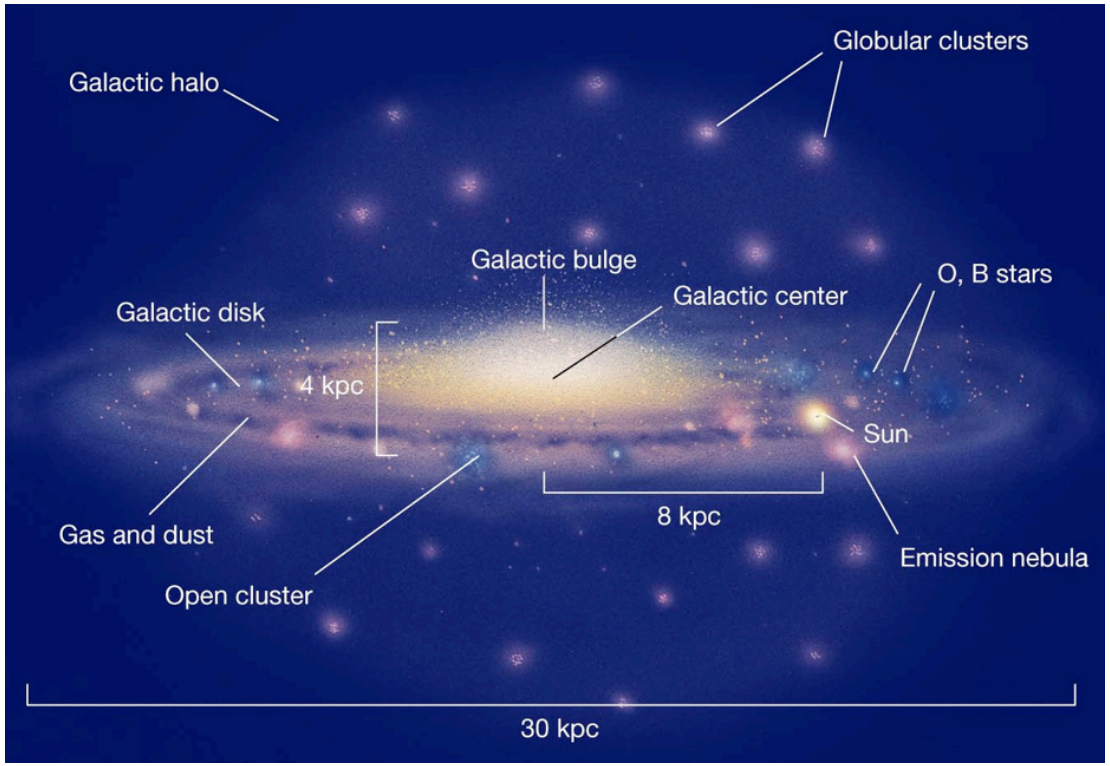

Dwarf Spheroidal Galaxy

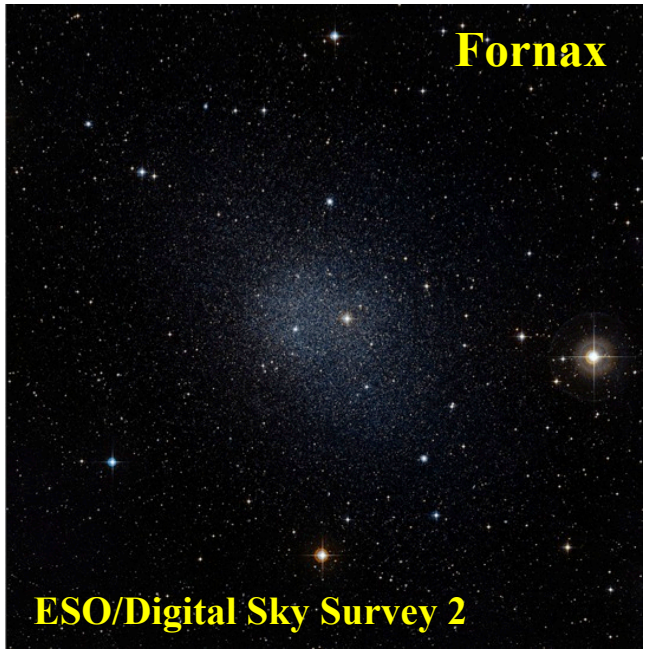

- **Galactic Center** (large astrophysical background, best visible from Southern Hemisphere)
- **Galactic Halo**
- **Galaxy Clusters & Globular Clusters**
- **Dwarf Spheroidal galaxies**

} **ideal candidates for MAGIC**

DM Searches with MAGIC

- **Dwarf Spheroidal galaxies: are among the most Dark Matter dominated structures in the Universe**

  They represent one of the best trade-off between:

  - large values of the J-factor & reduced uncertainties associated to the DM profiles

  - reduced gamma-ray contamination of astrophysical origin (no star formation)

→ Ideal for Dark Matter Annihilation searches

- **Galaxy Clusters: largest & most massive gravitationally bound systems in the Universe. Total masses 10^{14} - 10^{15} $M_{\odot}$ (5% galaxies, 15% gas & 80% dark matter)**

→ Ideal for Dark Matter Decay searches

MAGIC Dark Matter Searches: Mono mode (Single Telescope)

Best mono constrains come from Segue I

Galactic Center

(17 h): ApJ Lett. 638 (2006) L101

Galaxy Clusters

Perseus (25 h): ApJ 710 (2010) 634

Dwarf Spheroidals

Segue I (30 h): JCAP 06 (2011) 035

Willman I (16 h): ApJ 696 (2009) 1299

Draco (8 h): ApJ 679 (2008) 428

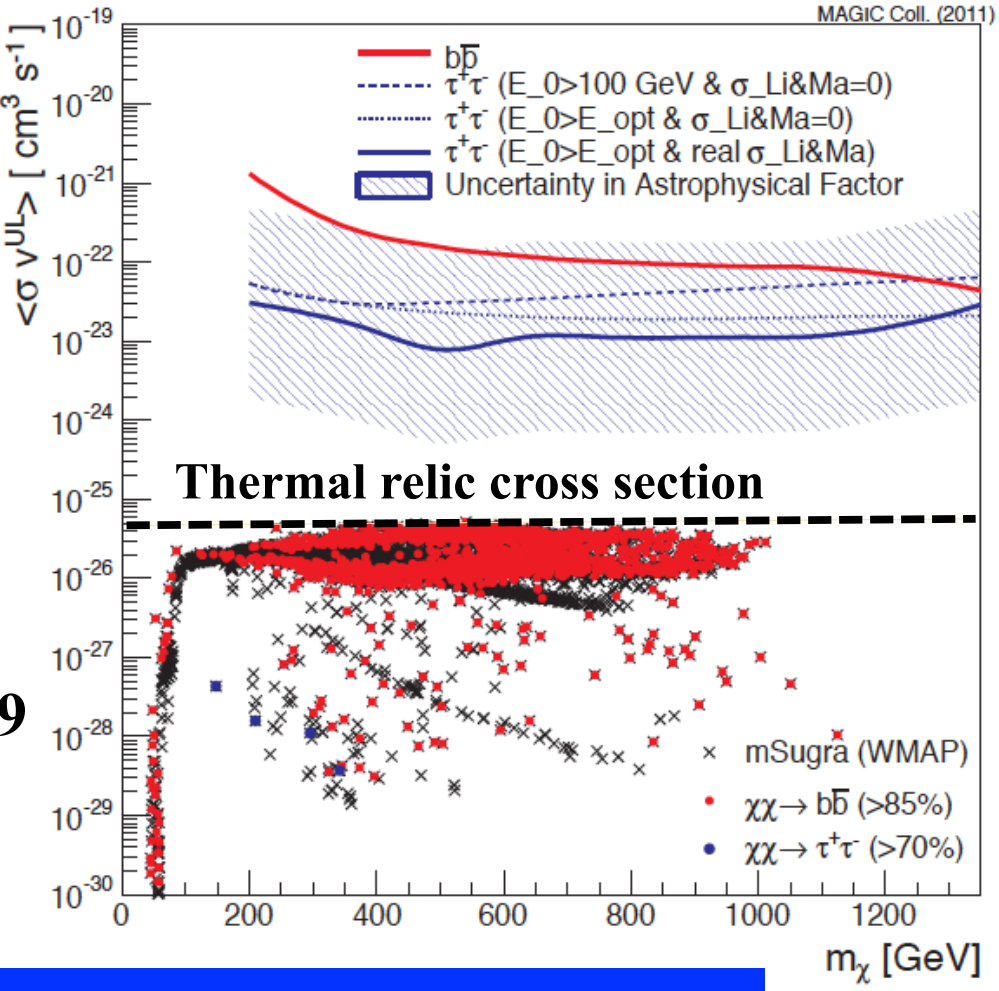

$\langle\sigma v\rangle \sim 10^{-22}$ cm^{3}s^{-1} excluded (m_{DM}= 1TeV to bb-bar)

DM Searches in Stereoscopic mode: Segue I

Dwarf Spheroidal Segue I	
Coordinates	$10^h\ 07^m\ 04^s$ $+16°\ 04'\ 55''$
Distance	23±2 kpc
Number of resolved stars	71
Magnitude	$-1.5^{+0.6}_{-0.8}$
Apparent magnitude	13.8±0.5
Luminosity	340 $L_\odot$
Mass	$5.8^{+8.2}_{-3.1} \times 10^5\ M_\odot$
M/L	~3400 $M_\odot/L_\odot$
Half-light radius	29^{+8}_{-5} pc
System velocity	208.5±0.9 km/s
Velocity dispersion	$3.7^{+1.4}_{-1.1}$ km/s
Mean [Fe/H]	-2.5

- One of the most dark matter dominated object known so far
- The least luminous galaxy
- Close by
- no astrophysical background
- Northern Hemisphere

- 158 h of data taken between January 2011-February 2013

Longest observation of a dSph with Cherenkov Telescopes

Segue I: Dark Matter annihilation with secondary photons

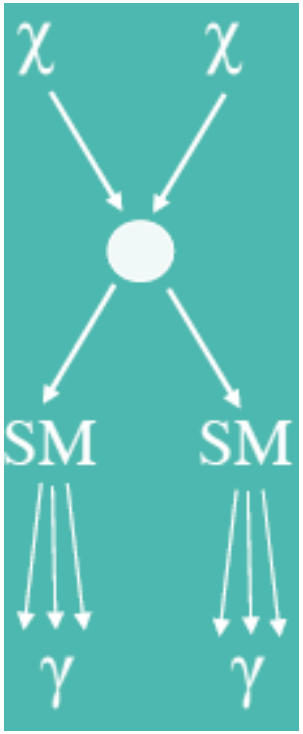

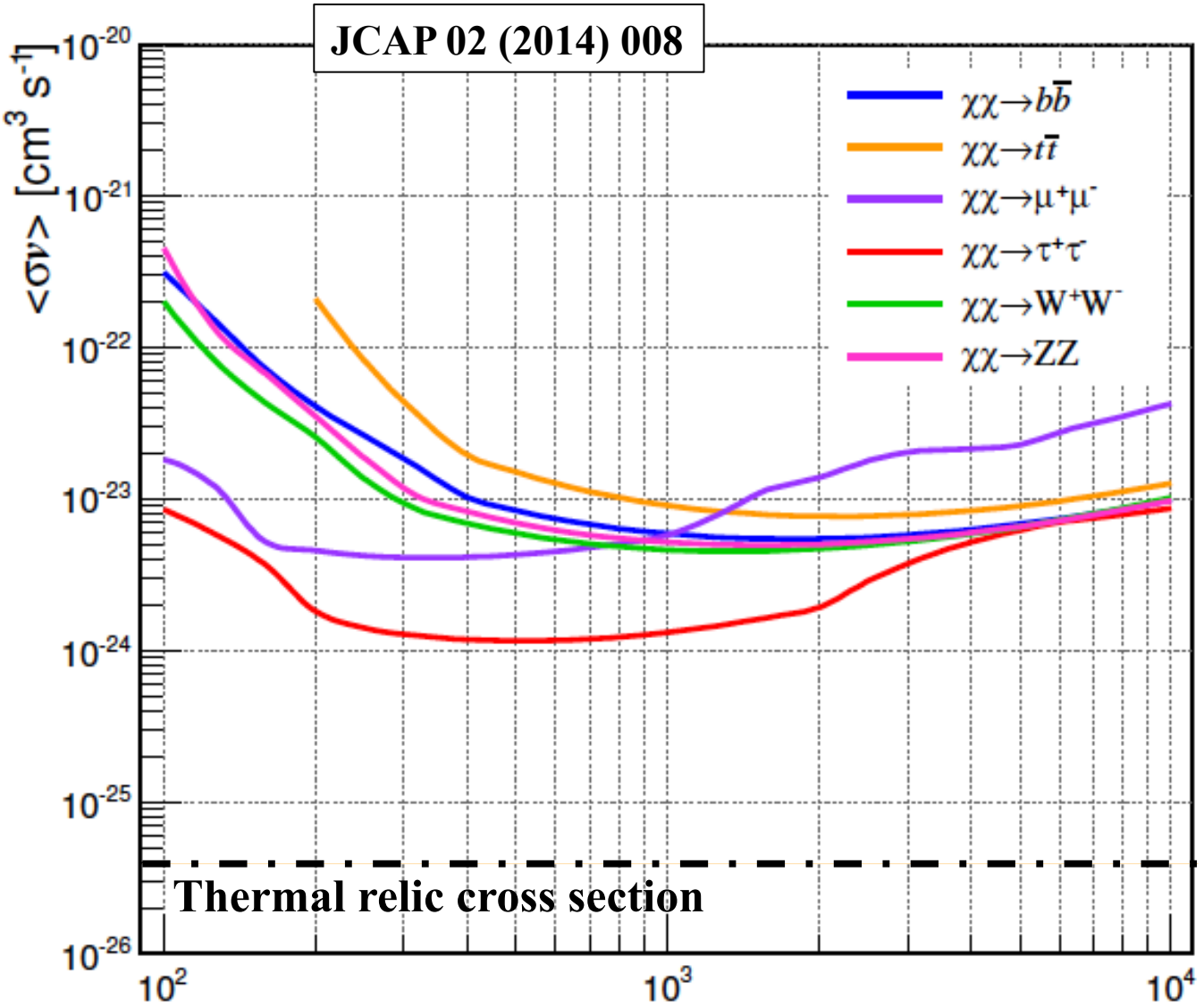

$\langle\sigma v\rangle \sim 10^{-23}$ cm^{3}s^{-1} excluded (m_{DM}= 1TeV to bb-bar)

Segue I: DM annihilation to b quarks

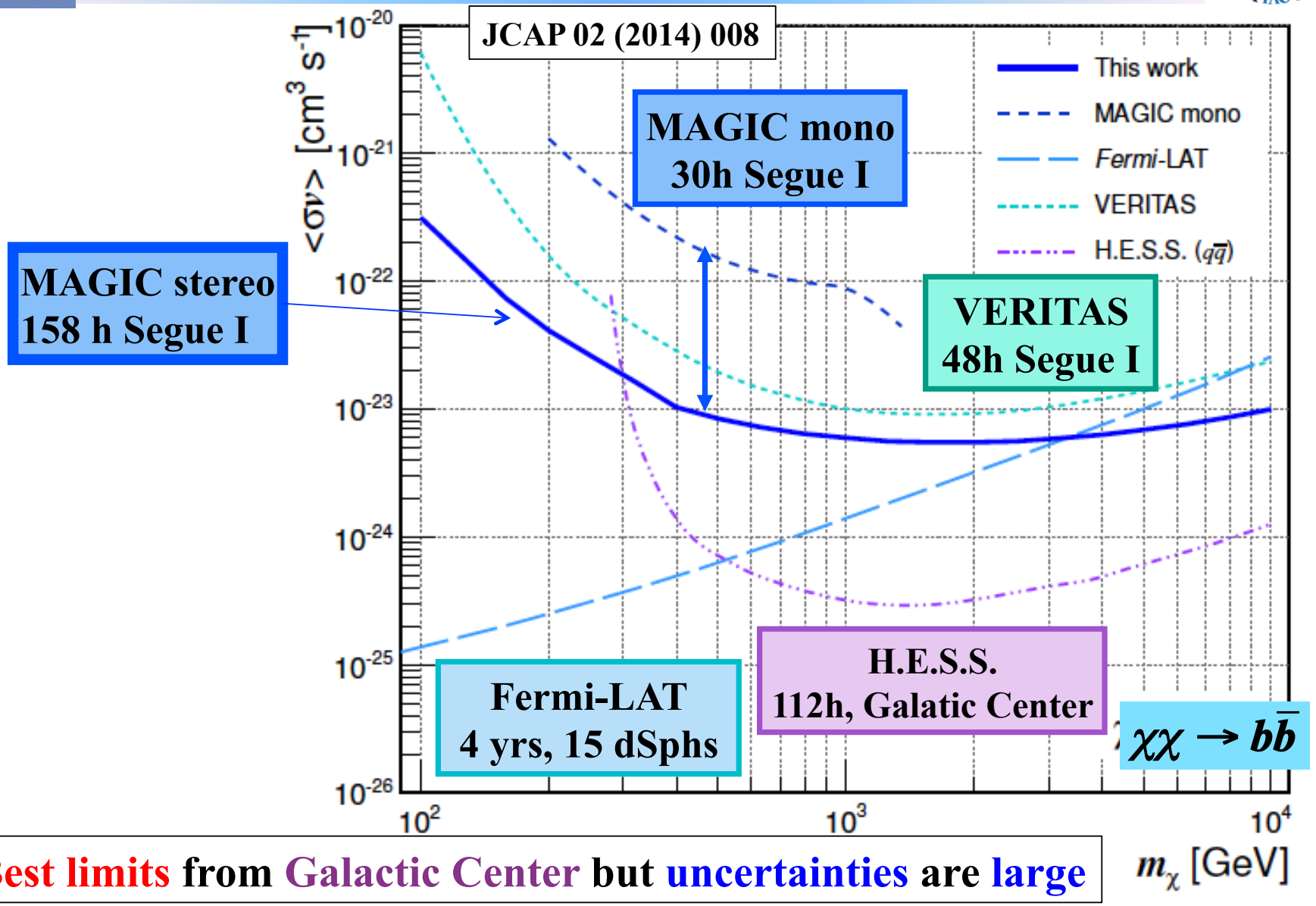

Best limits from **Galactic Center** but **uncertainties** are **large**

MAGIC + Fermi-LAT Dwarf Combination

JCAP 02 (2016) 039

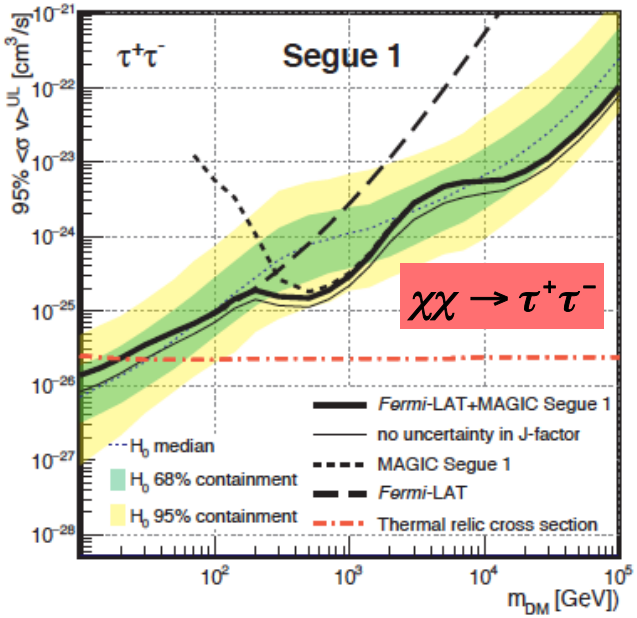

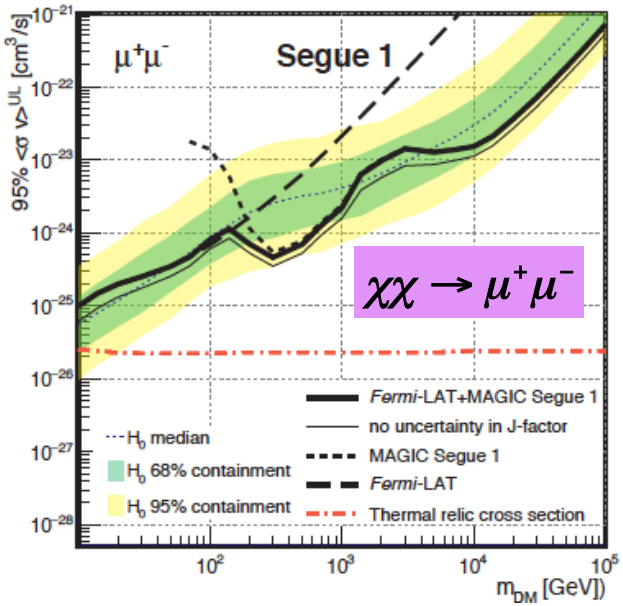

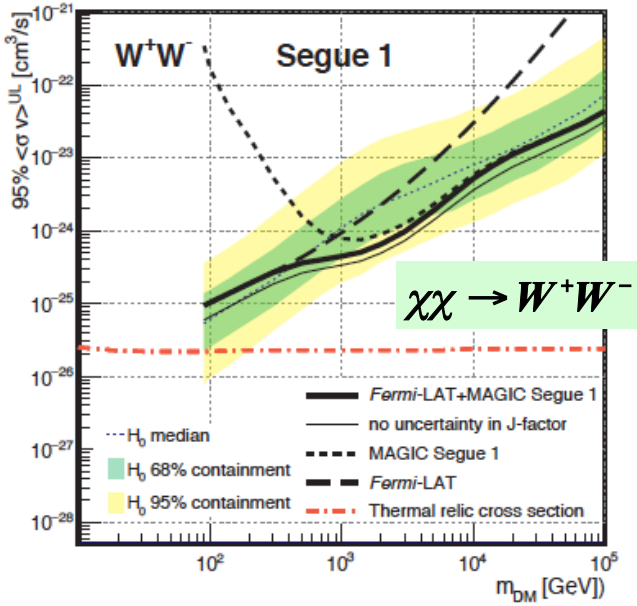

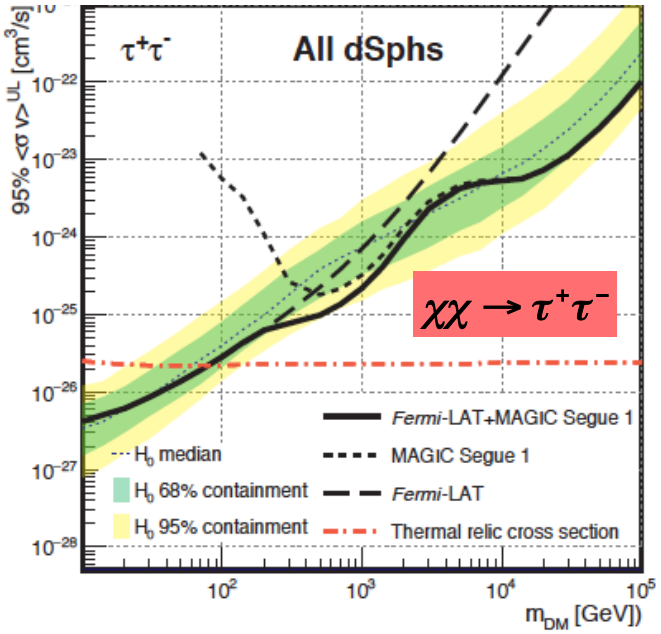

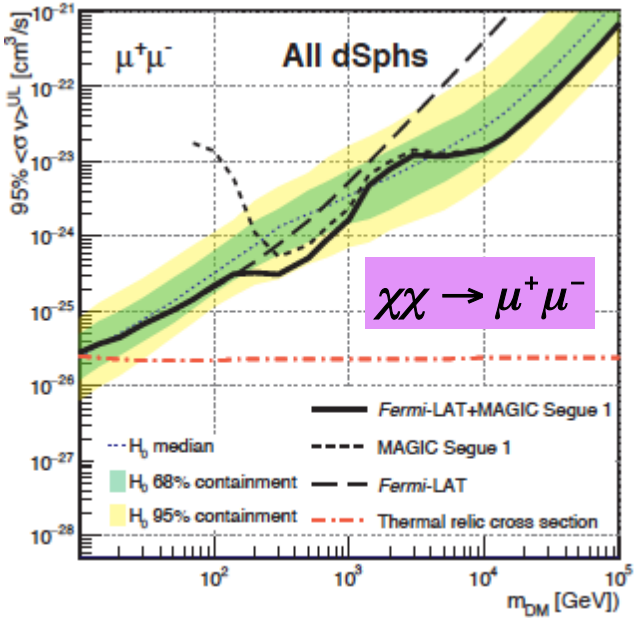

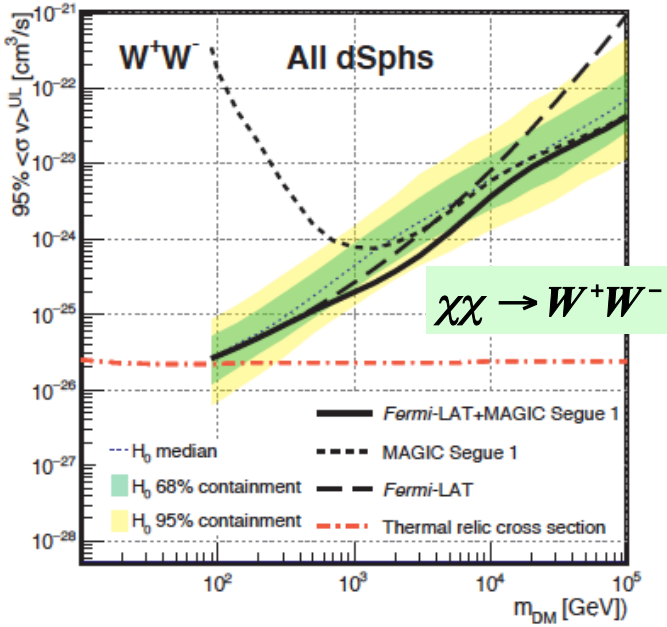

Segue I: Dark Matter Decay lifetime

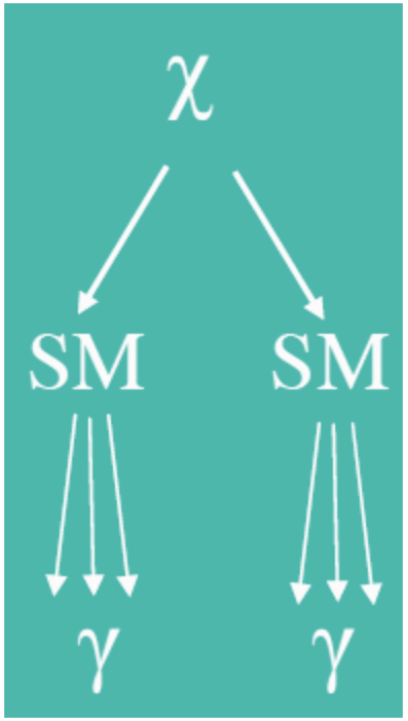

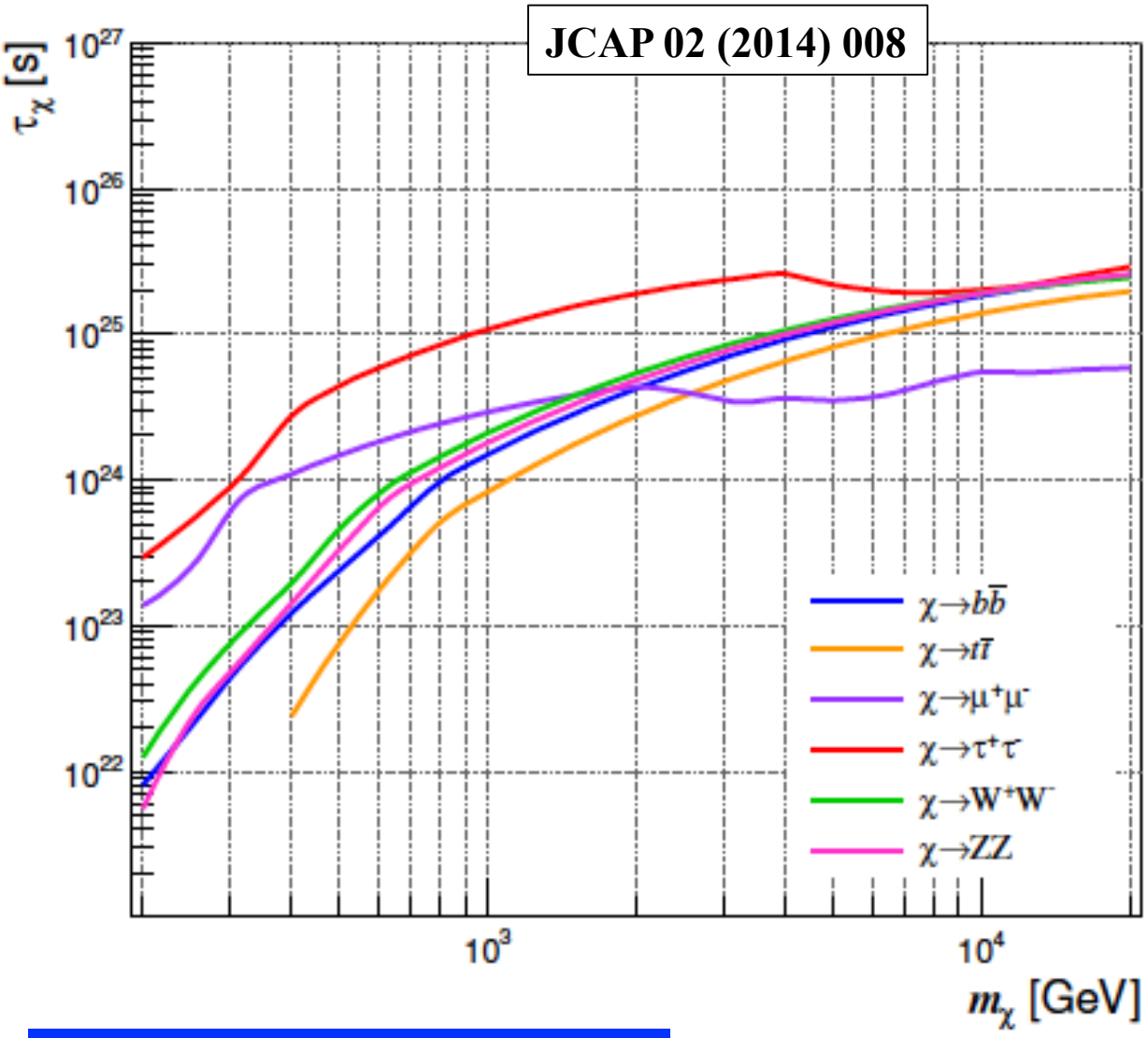

$\tau_\chi \leq 2 \cdot 10^{25}$ s excluded

Segue I: Dark Matter Decay into leptons

JCAP 02 (2014) 008

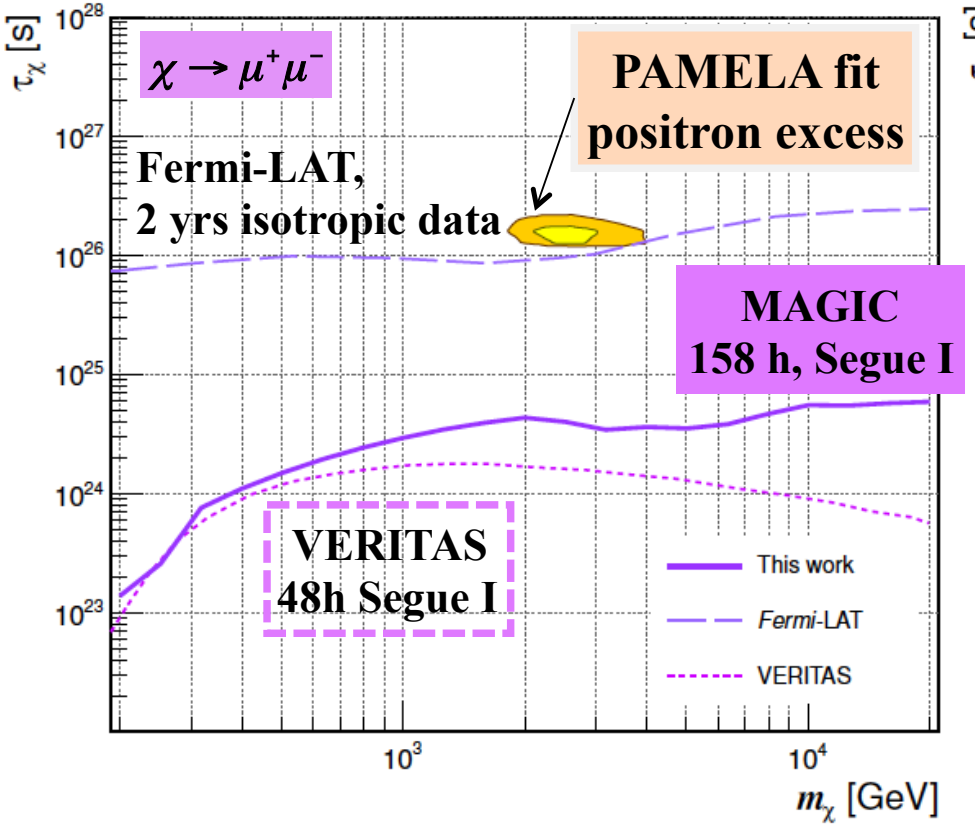

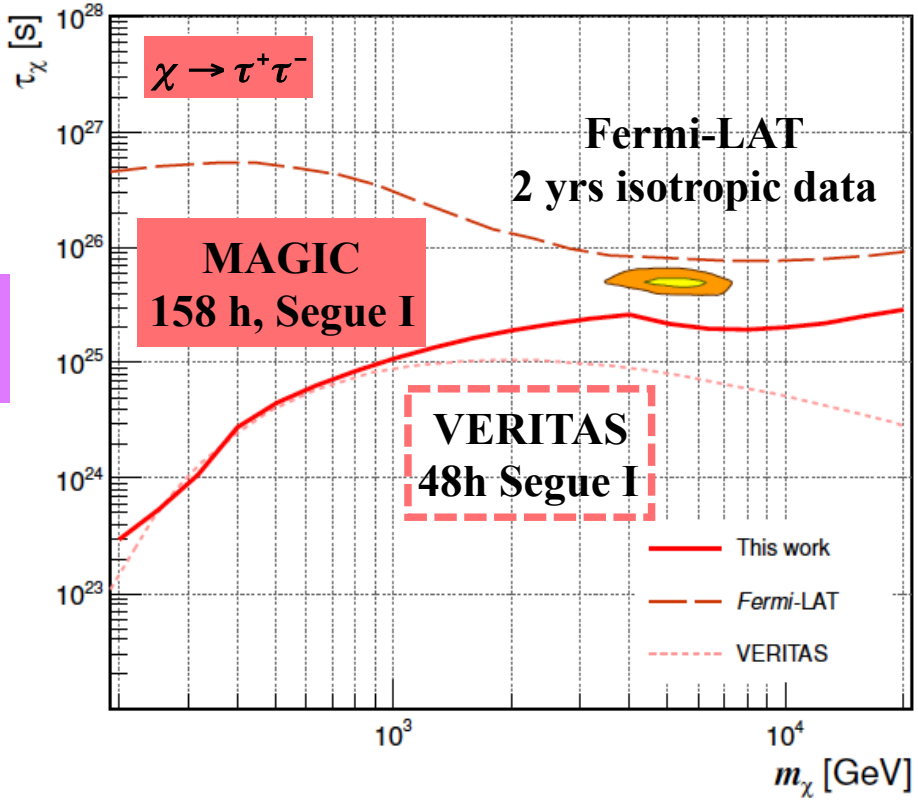

Strongest limits from Cherenkov Telescopes

Dwarfs are suboptimal targets for decaying dark matter searches

Search for DM in the Galaxy Cluster Perseus (Stereoscopic mode)

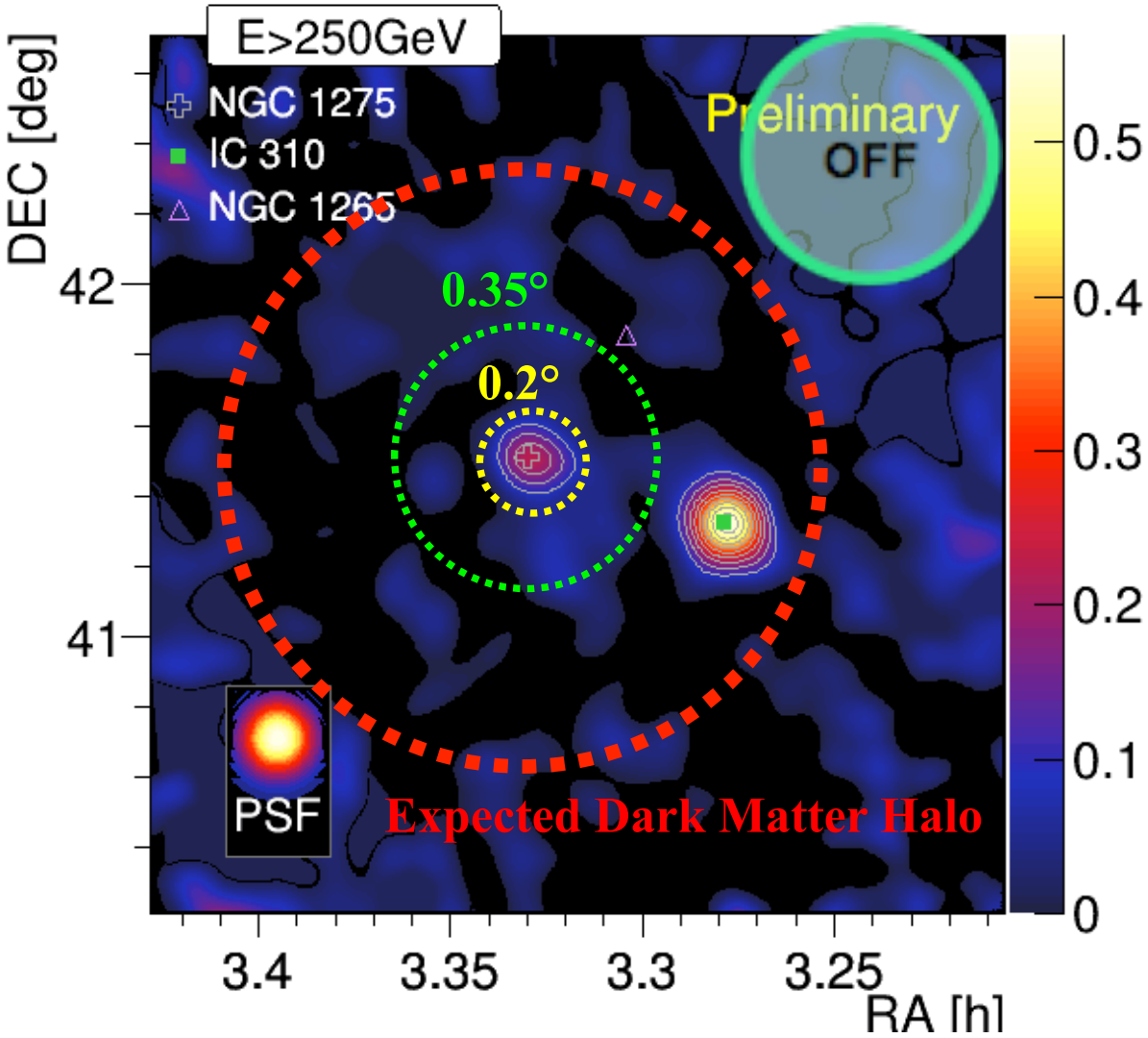

Search for DM in a ring:
$0.2° < \theta < 0.35°$
to avoid astrophysical contamination from NGC 1275

MAGIC has observed Perseus for ~ 250 h

First preliminary results with a sample of 12 h

→ **Ideal for Dark Matter Decay searches**

Perseus: Upper Limits on DM particle decay lifetime

Sensitive to $\tau \sim 8 \cdot 10^{25}$ seconds

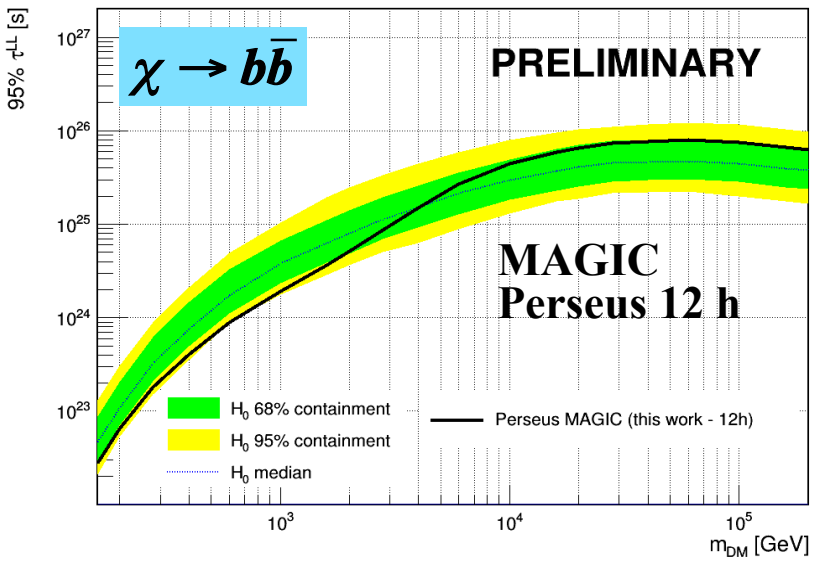

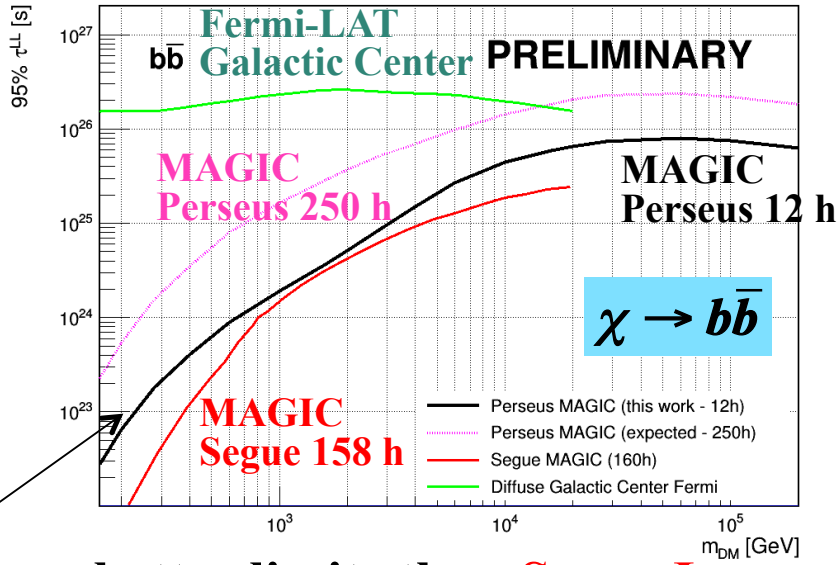

Perseus better limits than Segue I

Full dataset: expect factor 4 improvement

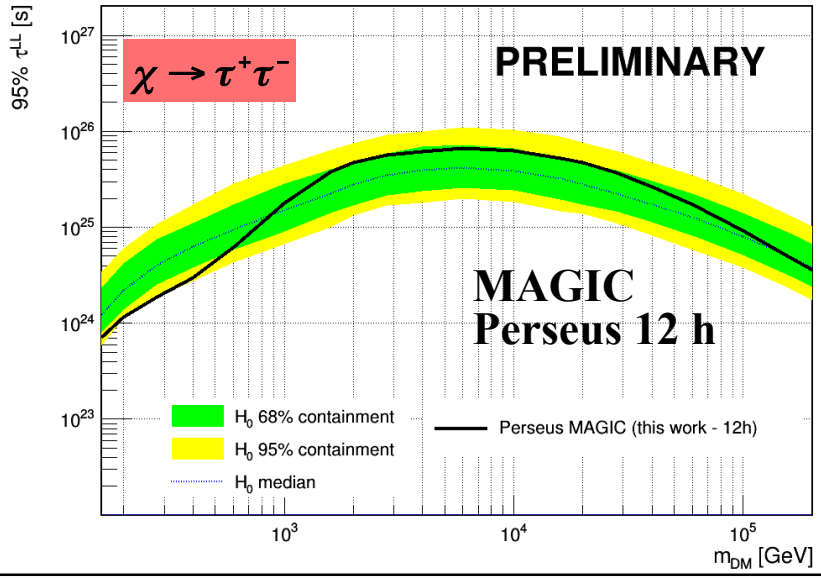

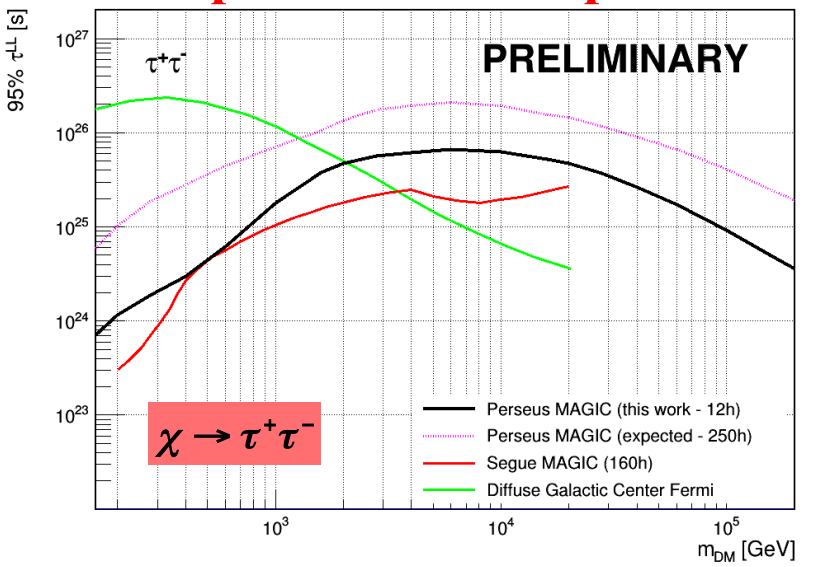

AMS positron excess

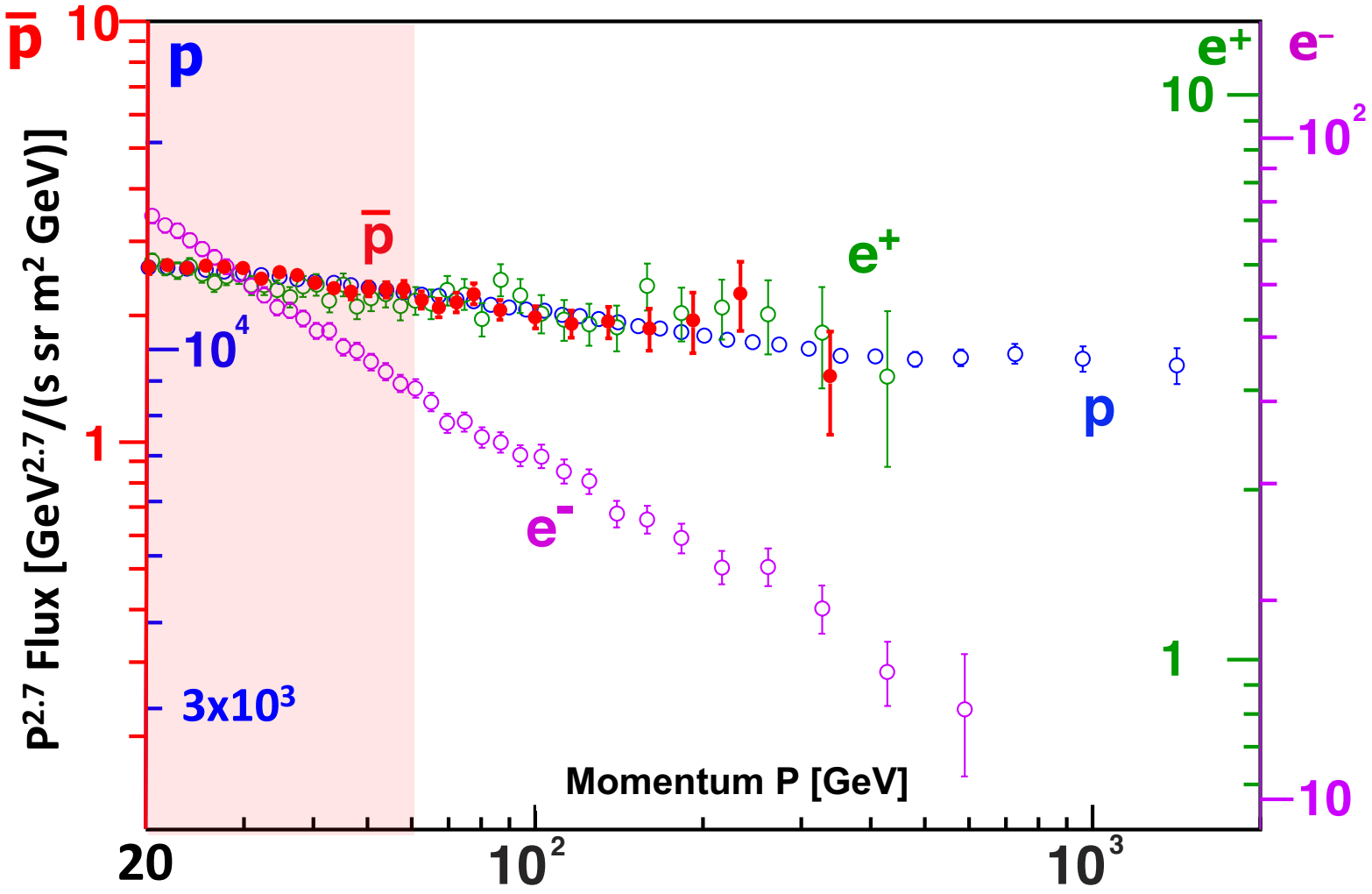

Figure 3. The positron, proton, and antiproton spectra have identical momentum dependence from 60 to 500 GeV. The electron spectrum exhibits a totally different behavior, it decreases much more rapidly with increasing momentum.

AMS positron excess

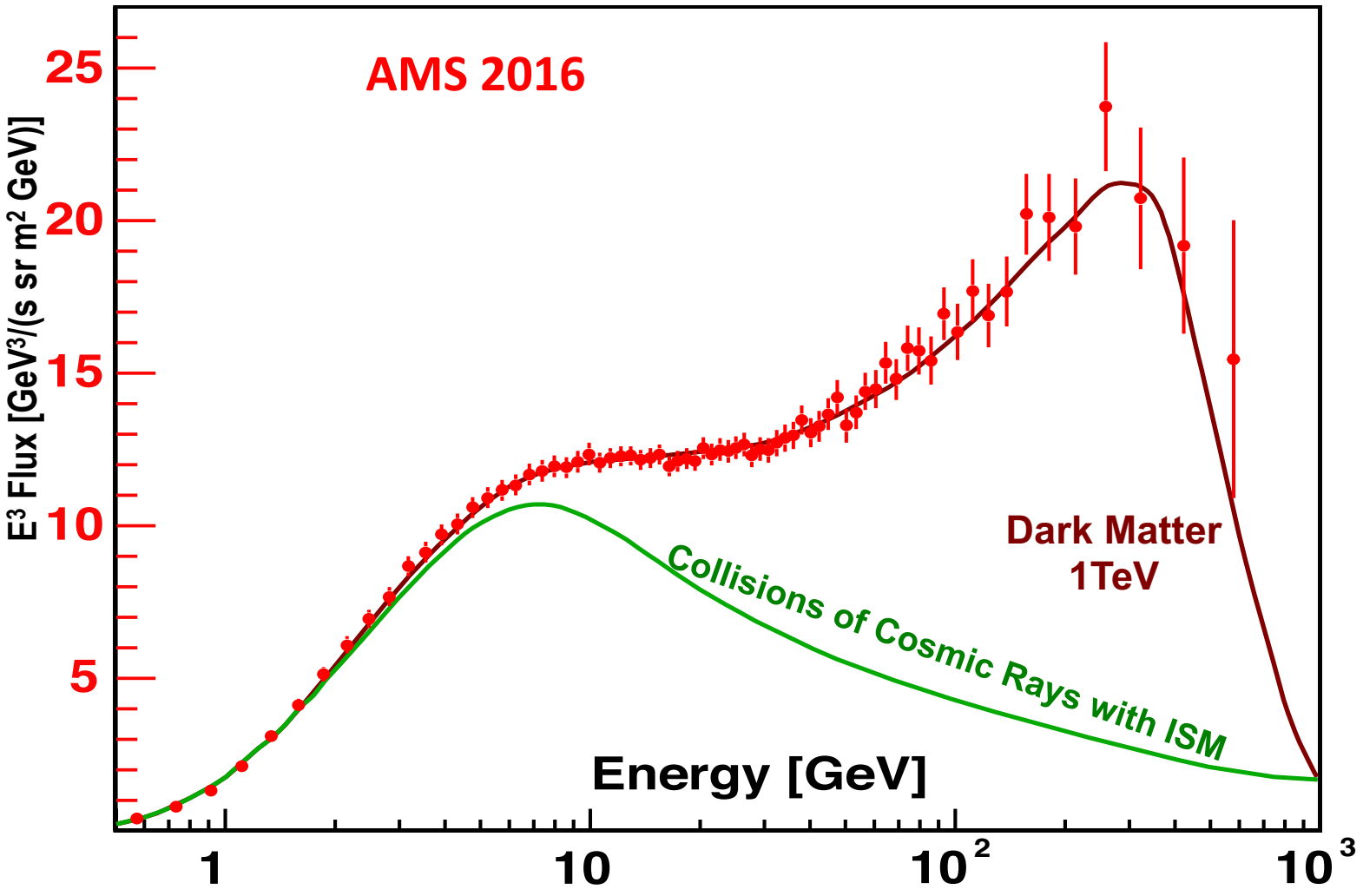

Figure 4. The current AMS positron flux measurement compared with theoretical models.

--> 1 TeV dark matter??

The origin of the positron excess in cosmic rays

Pasquale Blasi
INAF/Osservatorio Astrofisico di Arcetri, Largo E. Fermi, 5 50125 Firenze (Italy)
(Dated: May 10, 2009)

We show that the positron excess measured by the PAMELA experiment in the region between 10 and 100 GeV may well be a natural consequence of the standard scenario for the origin of Galactic cosmic rays. The 'excess' arises because of positrons created as secondary products of hadronic interactions inside the sources, but the crucial physical ingredient which leads to a natural explanation of the positron flux is the fact that the secondary production takes place in the same region where cosmic rays are being accelerated. Therefore secondary positrons (and electrons) participate in the acceleration process and turn out to have a very flat spectrum, which is responsible, after propagation in the Galaxy, for the observed positron 'excess'. This effect cannot be avoided though its strength depends on the values of the environmental parameters during the late stages of evolution of supernova remnants.

We also stress that a contribution to this positron flux might come from a fraction of SNRs located in proximity of dense molecular clouds, where the target for *pp* collisions may be enhanced and the importance of the mechanism made more evident. These SNRs might also have sufficiently high surface brightness (despite the old age) to be detected by Fermi/LAT, provided the target density for *pp* interactions is large enough.

BUT: could also be conventional astrophysics

Gravitational Waves

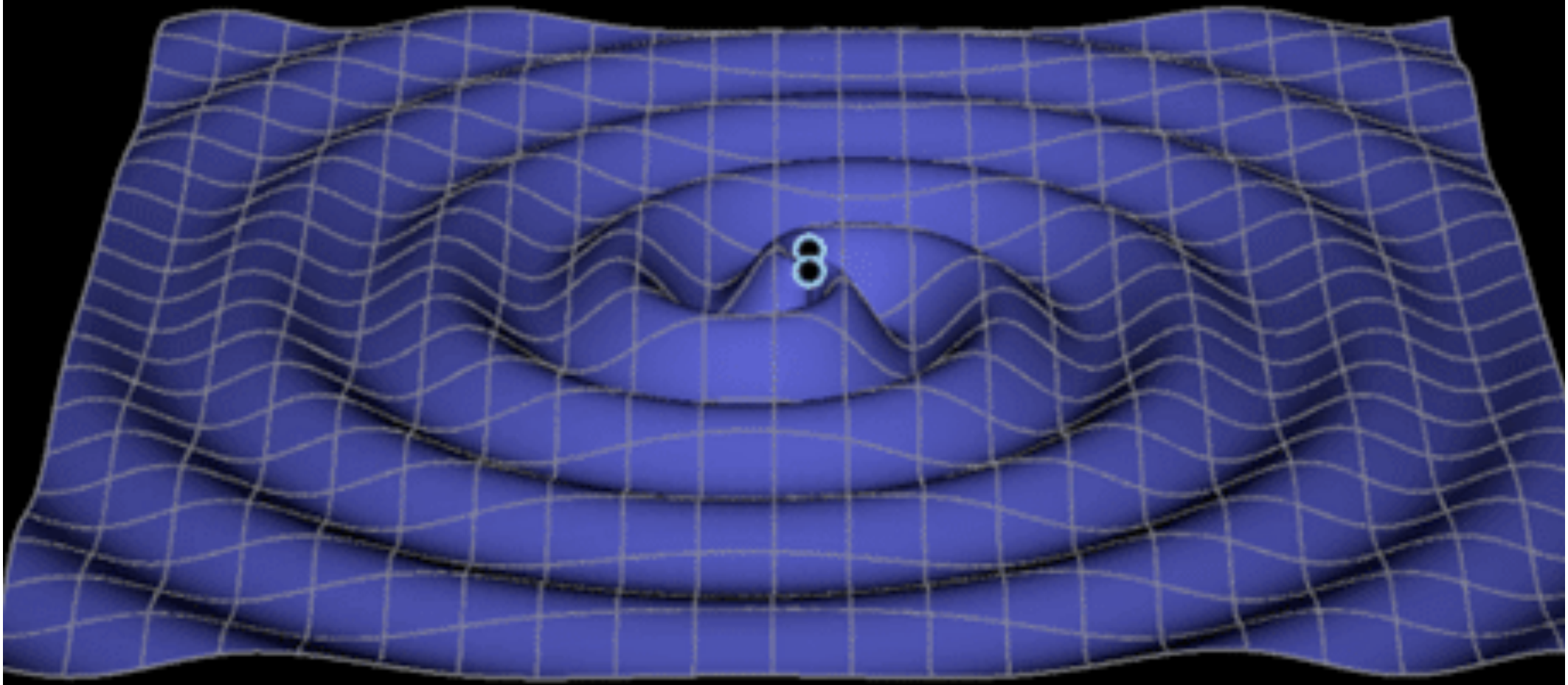

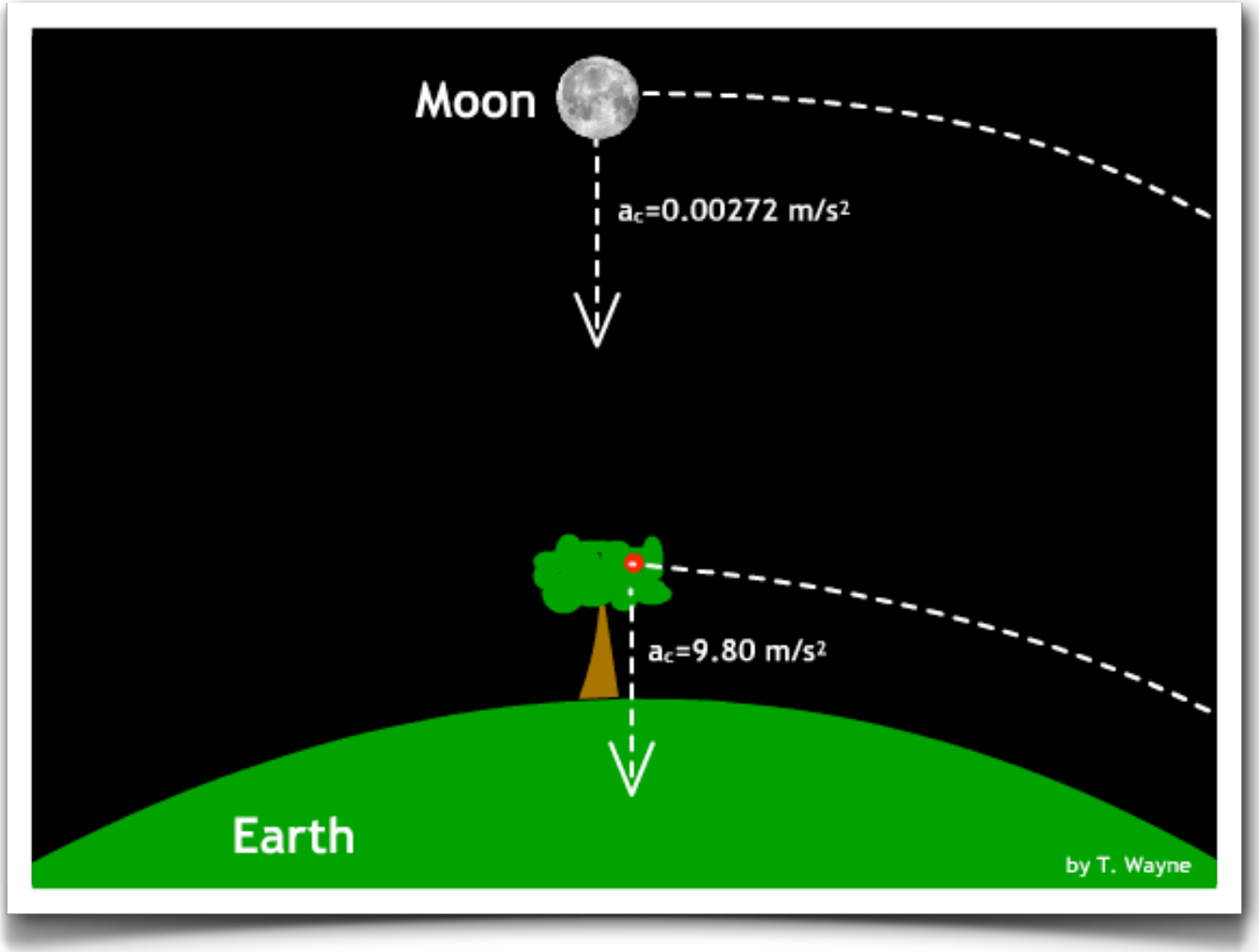

Isaac Newton
1642-1726

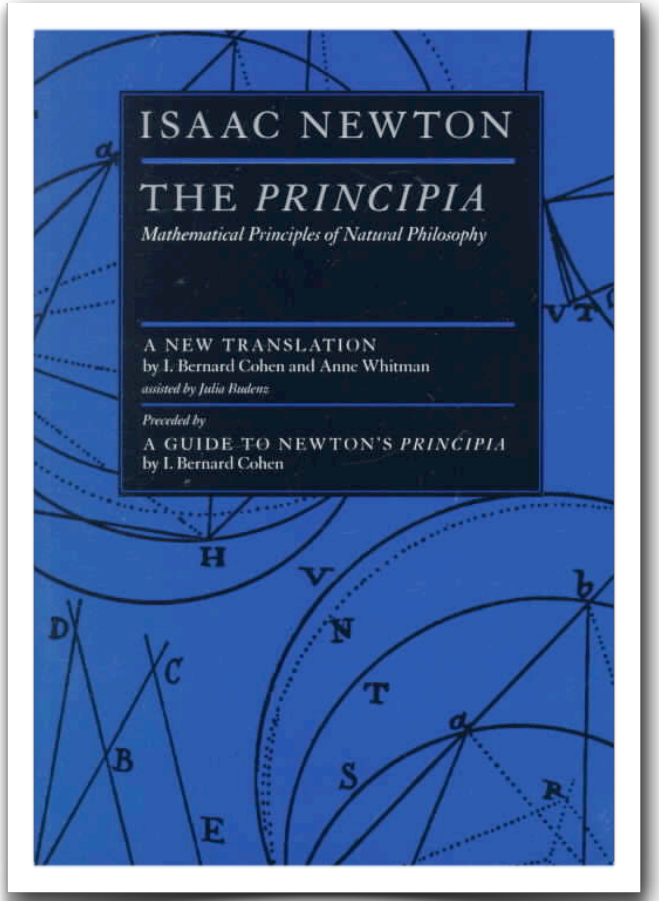

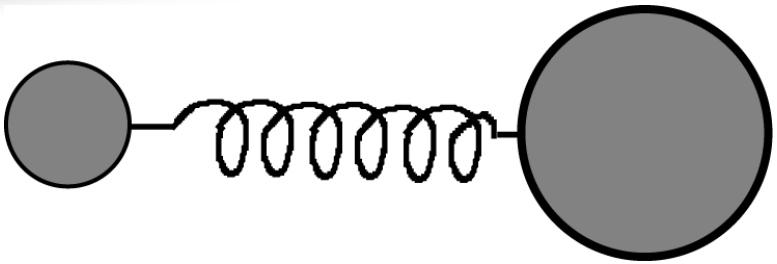

General Relativity

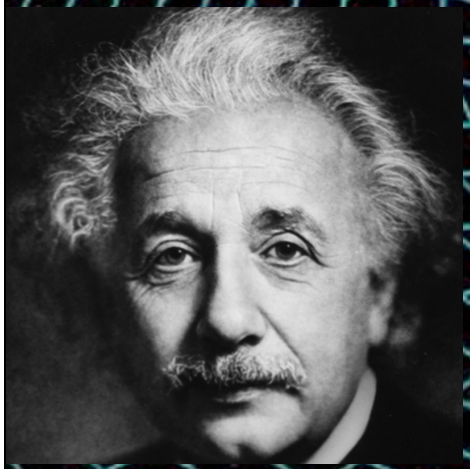

Albert Einstein
1879 - 1955

Einstein
field
equations

$$G_{\mu\nu} = \underbrace{\frac{8\pi\gamma}{c^4}}_{\approx 10^{-43}} T_{\mu\mu}$$

Newtonian vs General Relativistic gravity

Newtonian field equations	**GR field equations**
$\nabla^2\Phi = 4\,\pi G\rho$	$G^{ab} = \frac{8\pi G}{c^4} T^{ab}$
Source: mass density Gravitational field: scalar Φ	Source: energy-momentum tensor (includes mass densities/currents) Gravitational field: metric tensor g_{ab}

GWs: origins

- Electromagnetism: accelerating charges produce EM radiation.

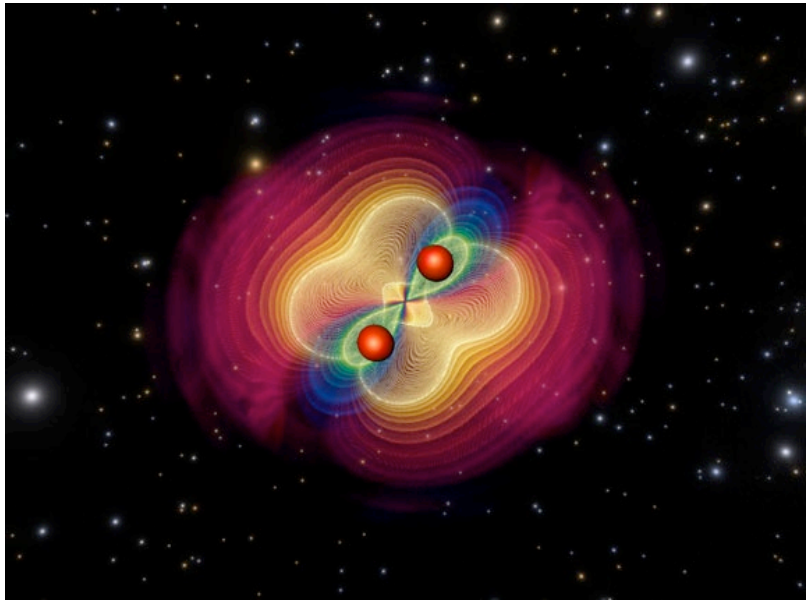

- Gravitation: accelerating masses produce gravitational radiation. (another hint: gravity has finite speed.)

GWs in linear gravity

- We consider weak gravitational fields:

$$g_{\mu\nu} \approx \eta_{\mu\nu} + h_{\mu\nu} + \mathcal{O}(h_{\mu\nu}^2)$$

↑ flat Minkowski metric

- The GR field equations in vacuum reduce to the standard wave equation:

$$\left(\frac{\partial^2}{\partial t^2} - \nabla^2 \right) h^{\mu\nu} = \Box h^{\mu\nu} = 0$$

- Comment: GR gravity like electromagnetism has a "gauge" freedom associated with the choice of coordinate system. The above equation applies in the so-called "transverse-traceless (TT)" gauge where

$$h_{0\mu} = 0, \qquad h^{\mu}_{\mu} = 0$$

Wave solutions

- Solving the previous wave equation in weak gravity is easy. The solutions represent “plane waves”:

$$h_{\mu\nu} = A_{\mu\nu} e^{i k_a x^a}$$

wave-vector

- Basic properties: $A_{\mu\nu} k^\mu = 0, \qquad k_a k^a = 0$

transverse waves

null vector = propagation along light rays

- Amplitude: $A^{\mu\nu} = h_+ e_+^{\mu\nu} + h_\times e_\times^{\mu\nu}$

two polarizations

GWs: polarization

- GWs come in two polarizations:

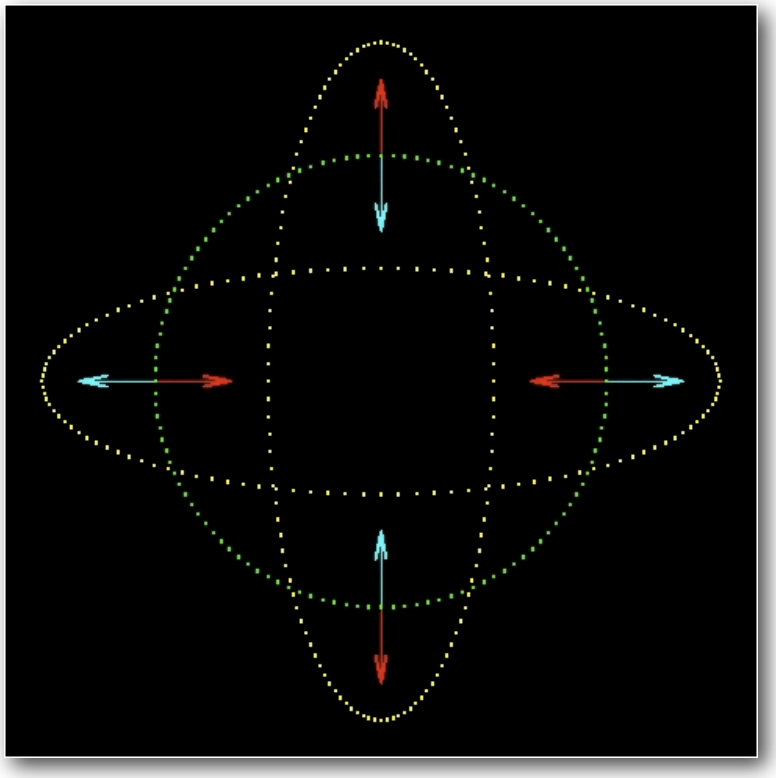

"+" polarization

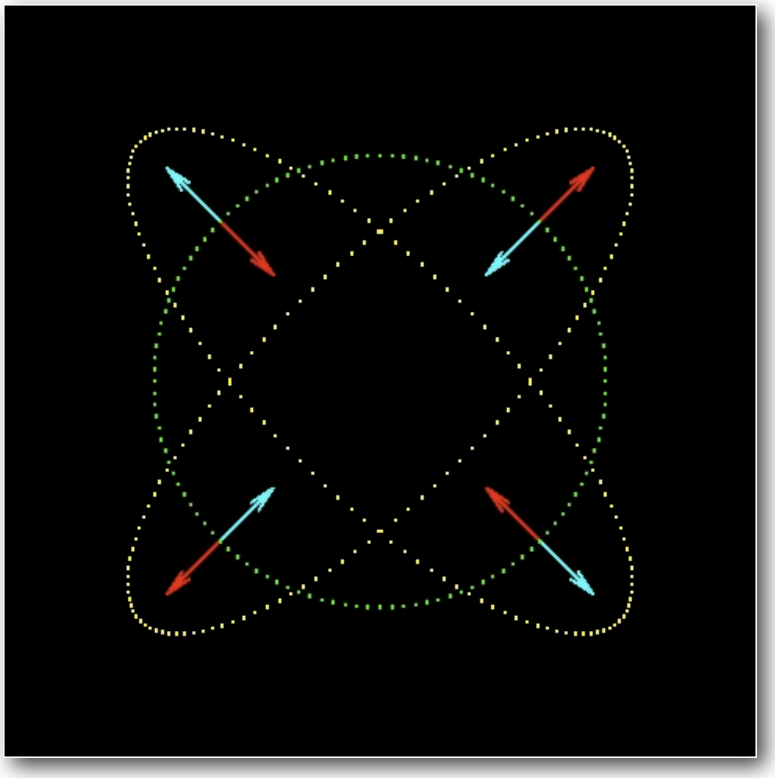

"x" polarization

GWs vs EM waves

- Similarities:

✓ Propagation with the speed of light.

✓ Amplitude decreases as ~ 1/r.

✓ Frequency redshift (Doppler, gravitational, cosmological).

- Differences:

✓ GWs propagate through matter with little interaction. Hard to detect, but they carry uncontaminated information about their sources.

✓ Strong GWs are generated by bulk (coherent) motion. They require strong gravity/high velocities (compact objects like black holes and neutron star).

✓ EM waves originate from small-scale, incoherent motion of charged particles. They are subject to “environmental” contamination (interstellar absorption etc.).

Part II

GW sources

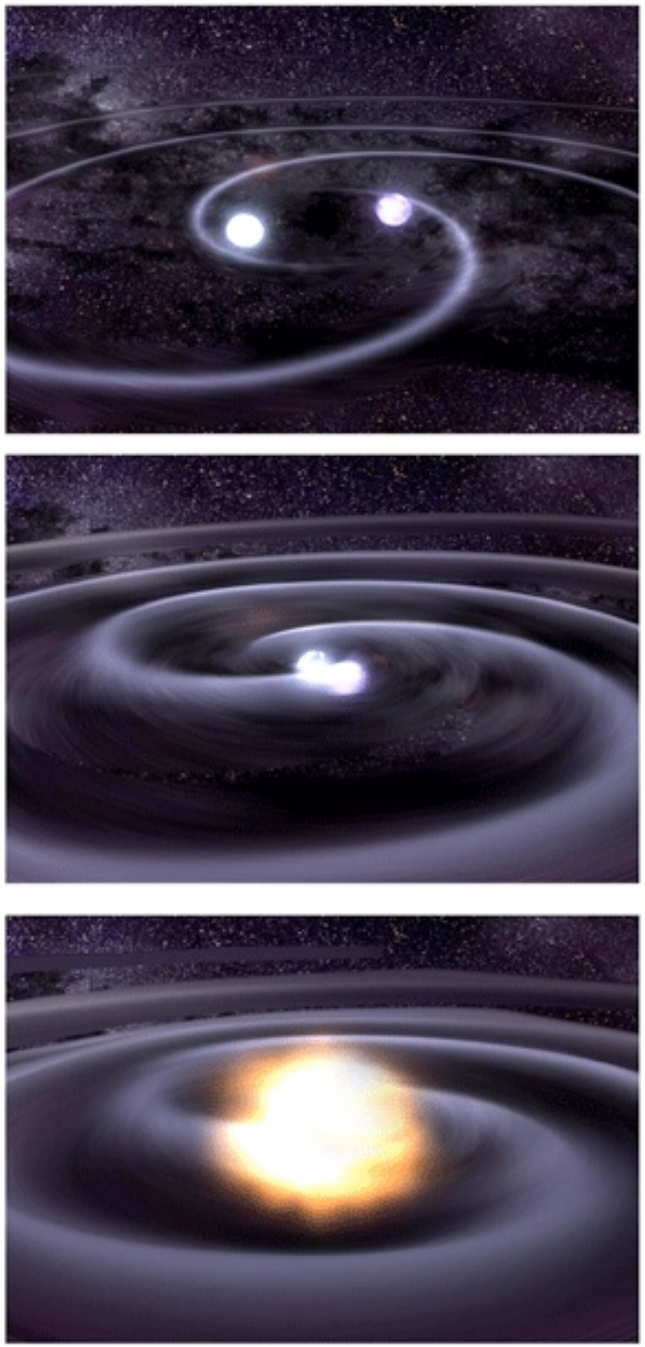

GW emission from a binary system (I)

- The binary consists of the two bodies M1 and M2 at distances a_1 and a_2 from the center of mass. The orbits are circular and lie on the x-y plane. The orbital angular frequency is Ω.

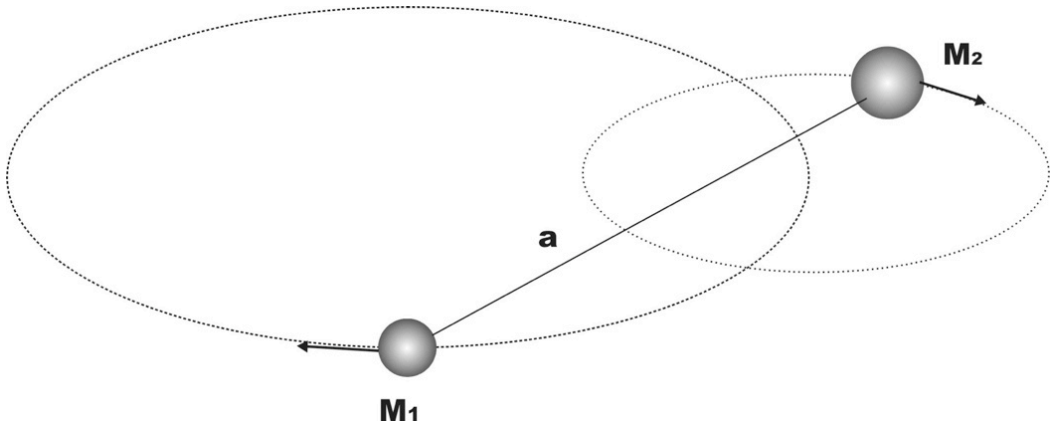

- We also define: $a = a_1 + a_2, \qquad \mu = M_1 M_2 / M, \qquad M = M_1 + M_2$

GW emission from a binary system (IV)

- In this analysis we have assumed circular orbits. In general the orbits can be elliptical, but it has been shown that GW emission circularizes them faster than the coalescence timescale.

- The GW amplitude is (ignoring geometrical factors):

$$h \approx 5 \times 10^{-22} \left(\frac{M}{2.8 M_\odot} \right)^{2/3} \left(\frac{\mu}{0.7 M_\odot} \right) \left(\frac{f}{100\,\mathrm{Hz}} \right)^{2/3} \left(\frac{15\,\mathrm{Mpc}}{r} \right)$$

PSR 1913+16: a Nobel-prize GW source

- The now famous Hulse & Taylor binary neutron star system provided the first astrophysical evidence of the existence of GWs !

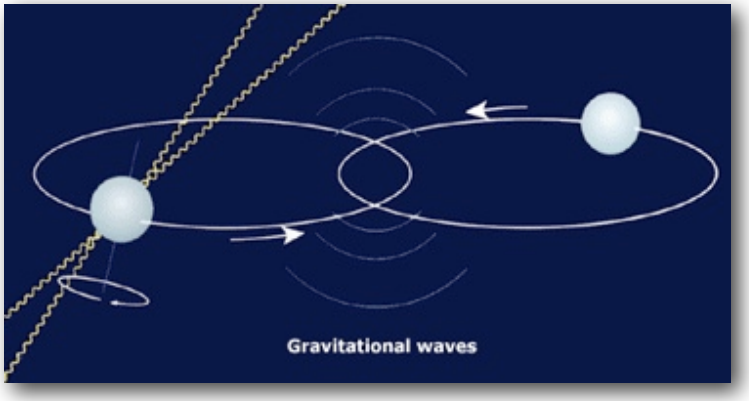

- The system's parameters: $r = 5\,\mathrm{Kpc}, \quad M_1 \approx M_2 \approx 1.4\,M_\odot, \quad T = 7\,\mathrm{h}\ 45\,\mathrm{min}$

- Using the previous equations we can predict:

$$\dot{T} = -2.4 \times 10^{-12}\,\mathrm{sec/sec}, \qquad f_{\mathrm{GW}} = 7 \times 10^{-5}\,\mathrm{Hz}, \qquad h \sim 10^{-23}, \quad \tau \approx 3.5 \times 10^{8}\,\mathrm{yr}$$

Theory vs observations

- How can the orbital parameters be measured with such high precision?
- One of the neutron stars is a pulsar, emitting extremely stable periodic radio pulses. The emission is modulated by the orbital motion.
- Since the discovery of the H-T system in 1974 more such binaries were found by astronomers.

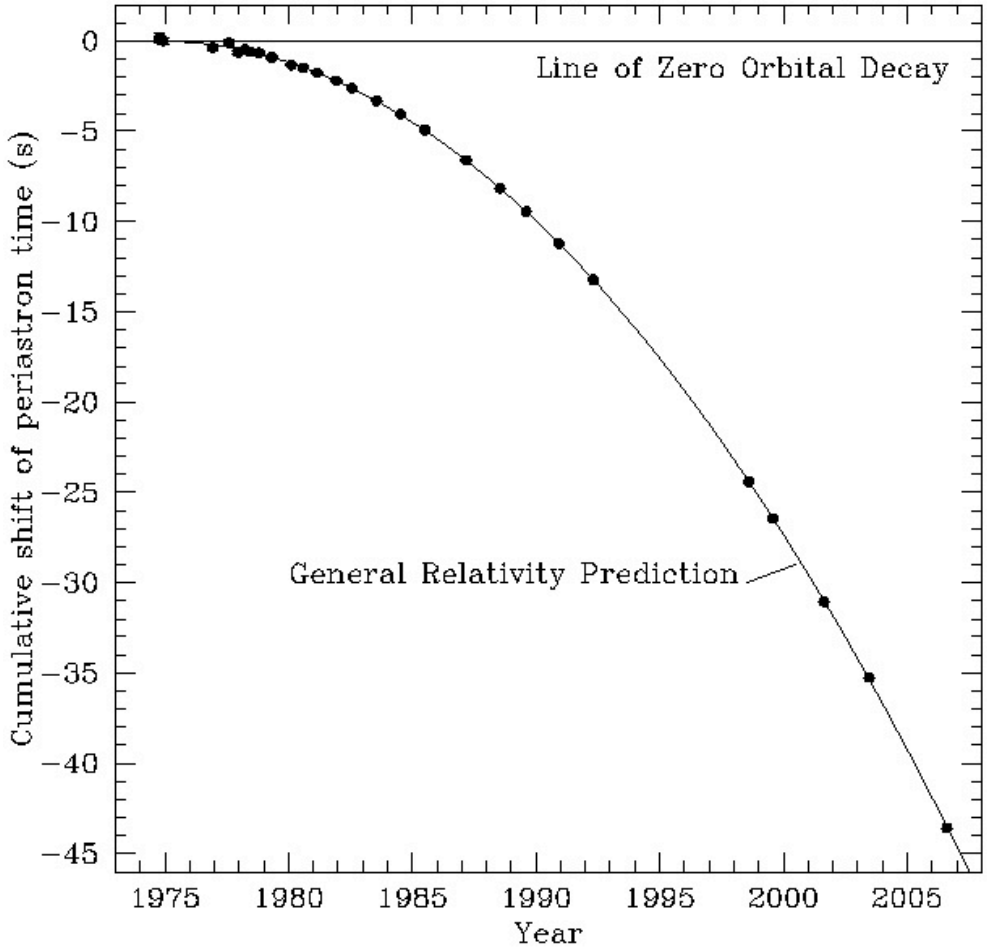

Part III

Detection of GWs

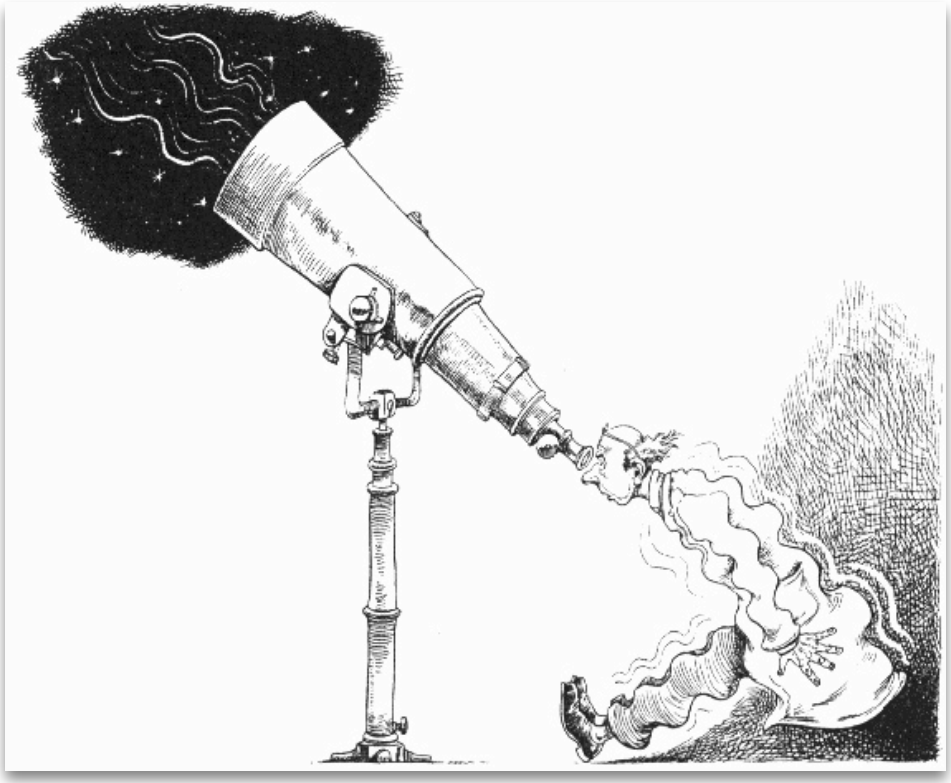

GW detectors: prehistory

- For decades after the formulation of Einstein's GR the notion of GWs was a topic for speculations and remote from real astrophysics.

- Joe Weber pioneered the construction of the first "primitive" bar detector. However, his claims of a GW detection were never verified ...

- Theoretical work in the 1970s-1990s (and the discovery of the Hulse-Taylor pulsar) advanced the popularity of GWs.

- GW astronomy is expected to become reality in the present decade.

A toy model GW detector

- Consider a GW propagating along the z-axis (with a "+" polarization and frequency ω), impinging on an idealized detector consisting of two masses joined by a spring (of length L) along the x-axis

- The resulting motion is that of a forced oscillator (with friction τ, natural frequency ω_0):

$$\ddot{\xi} + \dot{\xi}/\tau + \omega_0^2 \xi = -\frac{1}{2}\omega^2 L h_+ e^{i\omega t}$$

- The solution is:

$$\xi = \frac{\omega^2 L h_+}{2(\omega_0^2 - \omega^2 + i\omega/\tau)} e^{i\omega t}$$

- The maximum amplitude is achieved at $\omega \approx \omega_0$ and has a size: $\xi_{\max} = \frac{1}{2}\omega_0 \tau L h_+$

- The detector can be optimized by increasing $\omega_0 \tau L$.

Bar detectors

- Bar detectors are narrow bandwidth instruments (like the previous toy-model)

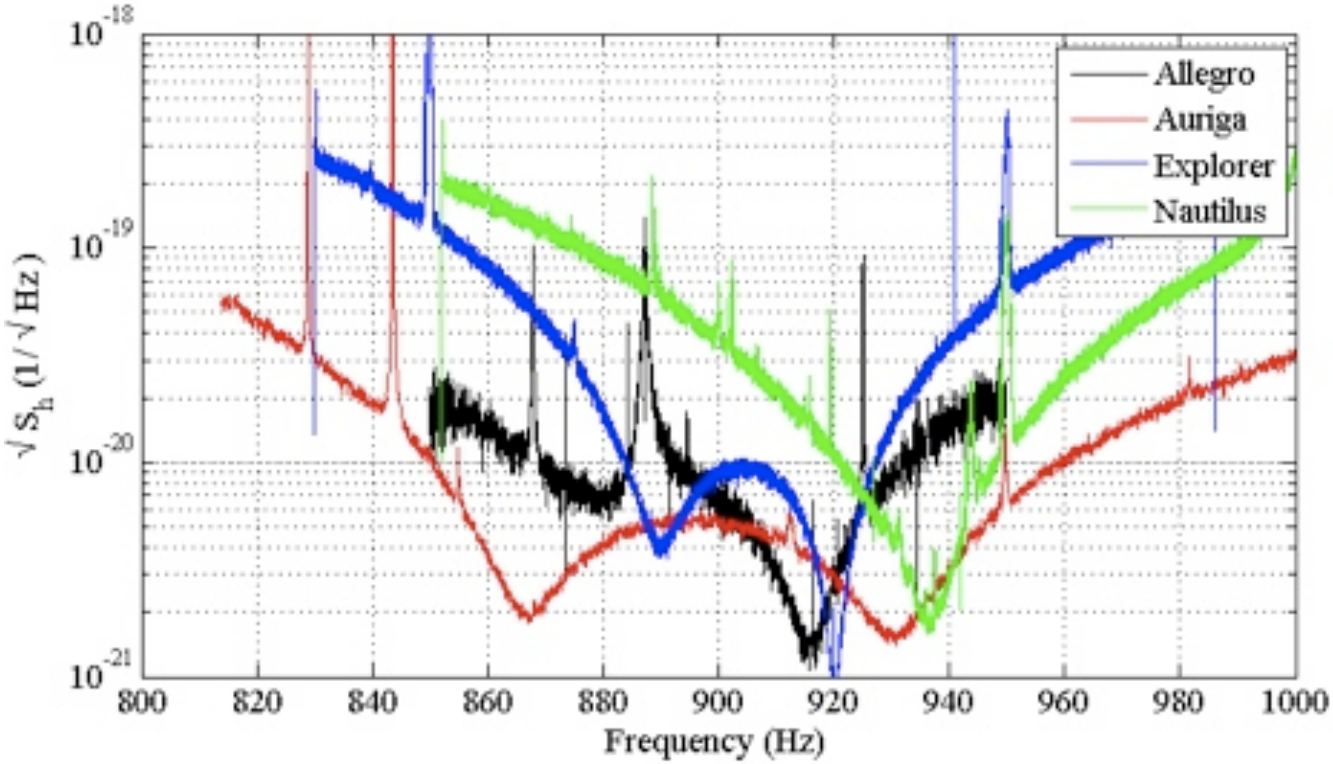

Sensitivity curves of various bar detectors

Detectors: laser interferometry

- A laser interferometer is an alternative choice for GW detection, offering a combination of very high sensitivities over a broad frequency band.

- Suspended mirrors play the role of “test-particles”, placed in perpendicular directions. The light is reflected on the mirrors and returns back to the beam splitter and then to a photodetector where the fringe pattern is monitored.

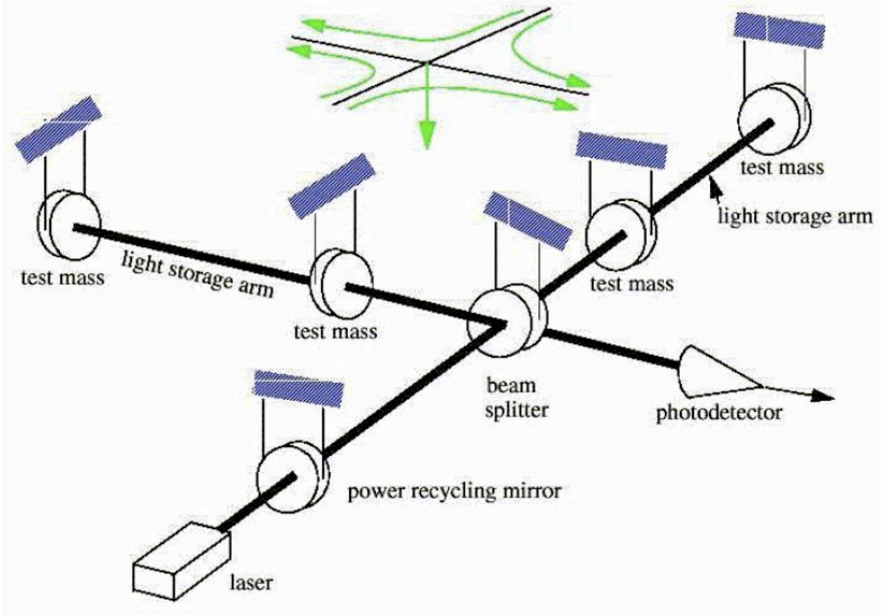

Noise in interferometric detectors

- Seismic noise (low frequencies). At frequencies below 60 Hz, the noise in the interferometers is dominated by seismic noise. The vibrations of the ground couple to the mirrors via the wire suspensions which support them. This effect is strongly suppressed by properly designed suspension systems. Still, seismic noise is very difficult to eliminate at frequencies below 5-10 Hz.

- Photon shot noise (high frequencies). The precision of the measurements is restricted by fluctuations in the fringe pattern due to fluctuations in the number of detected photons. The number of detected photons is proportional to the intensity of the laser beam. Statistical fluctuations in the number of detected photons imply an uncertainty in the measurement of the arm length.

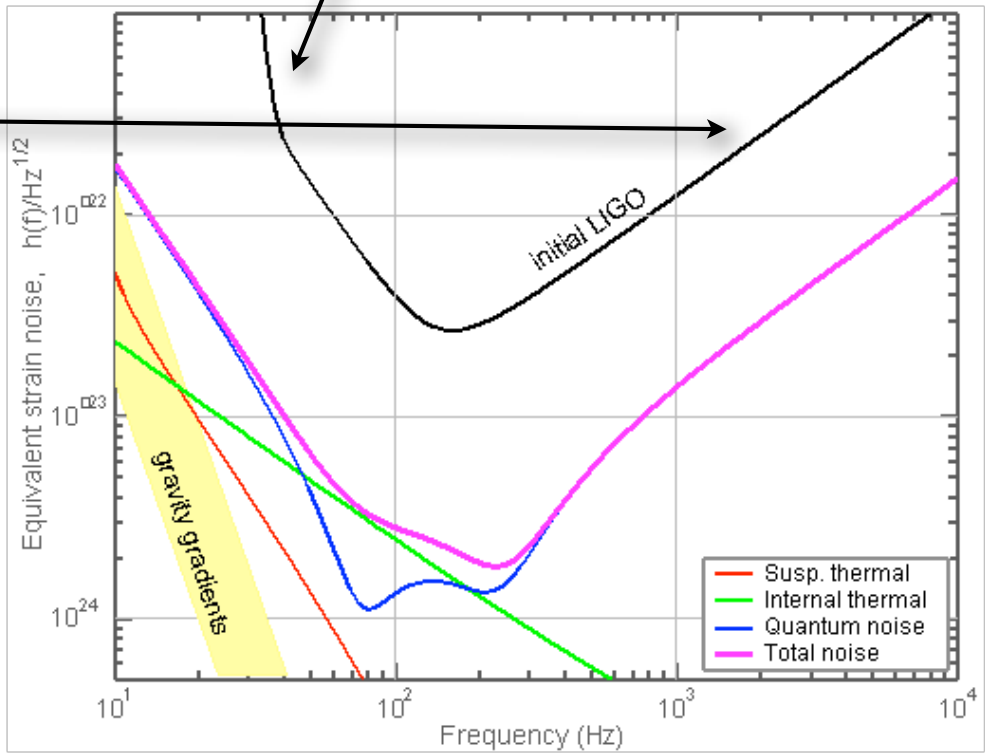

Detectors: real-life sensitivity

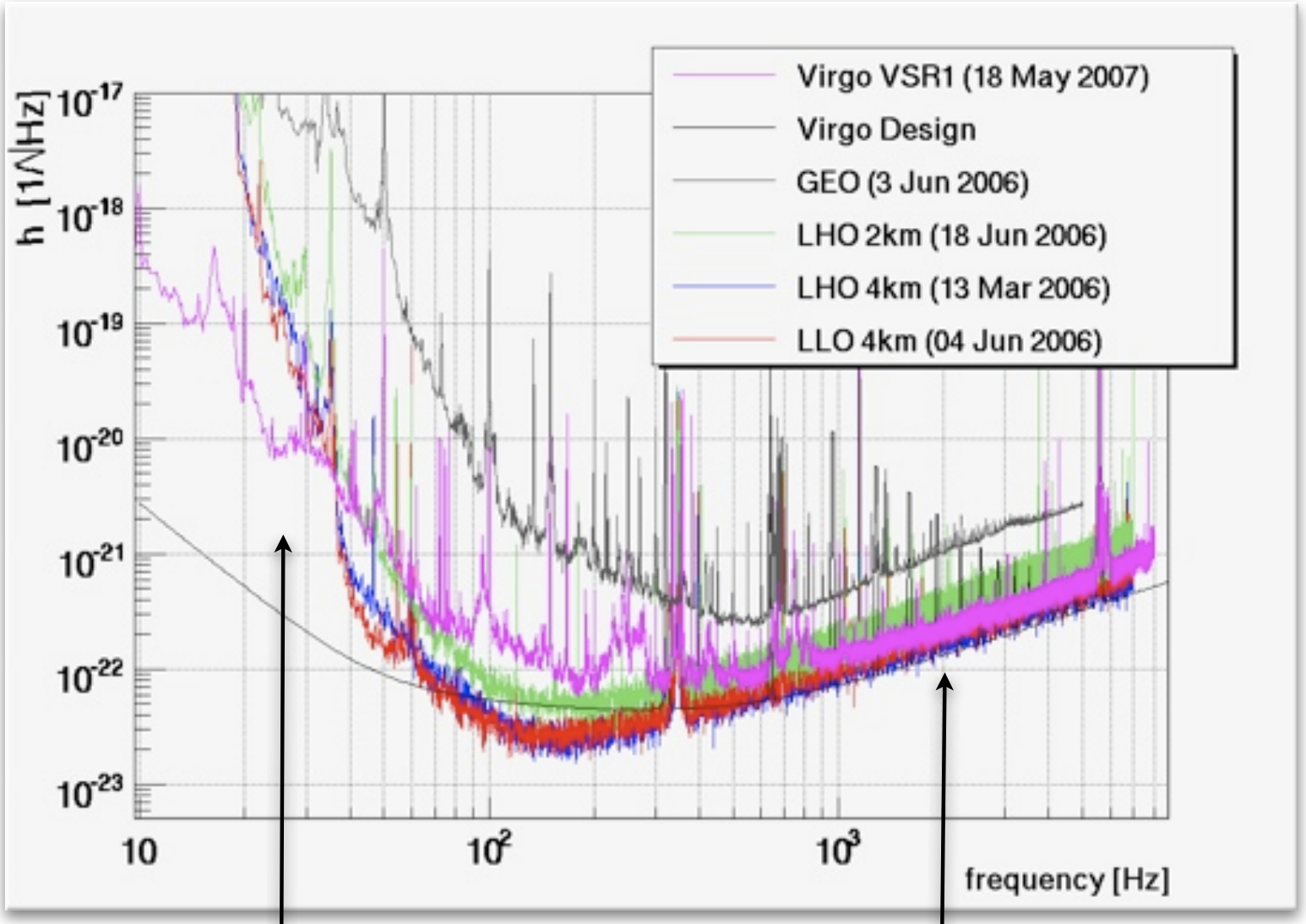

Seismic noise

laser photon noise

Detectors: the present (I)

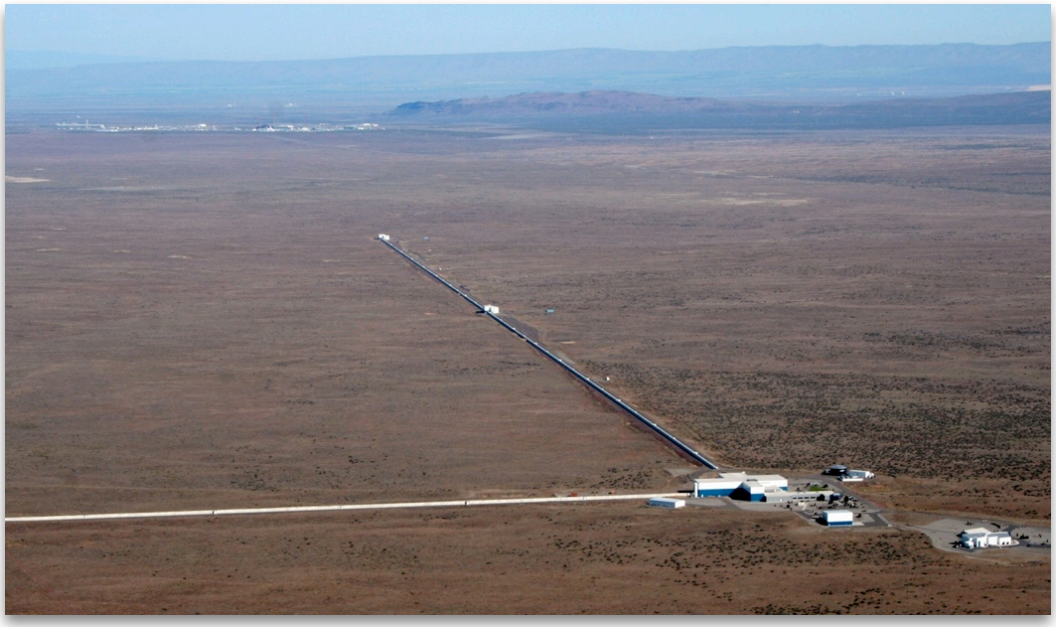

The twin LIGO detectors (L = 4 km) at Livingston Louisiana and Hanford Washington (US).

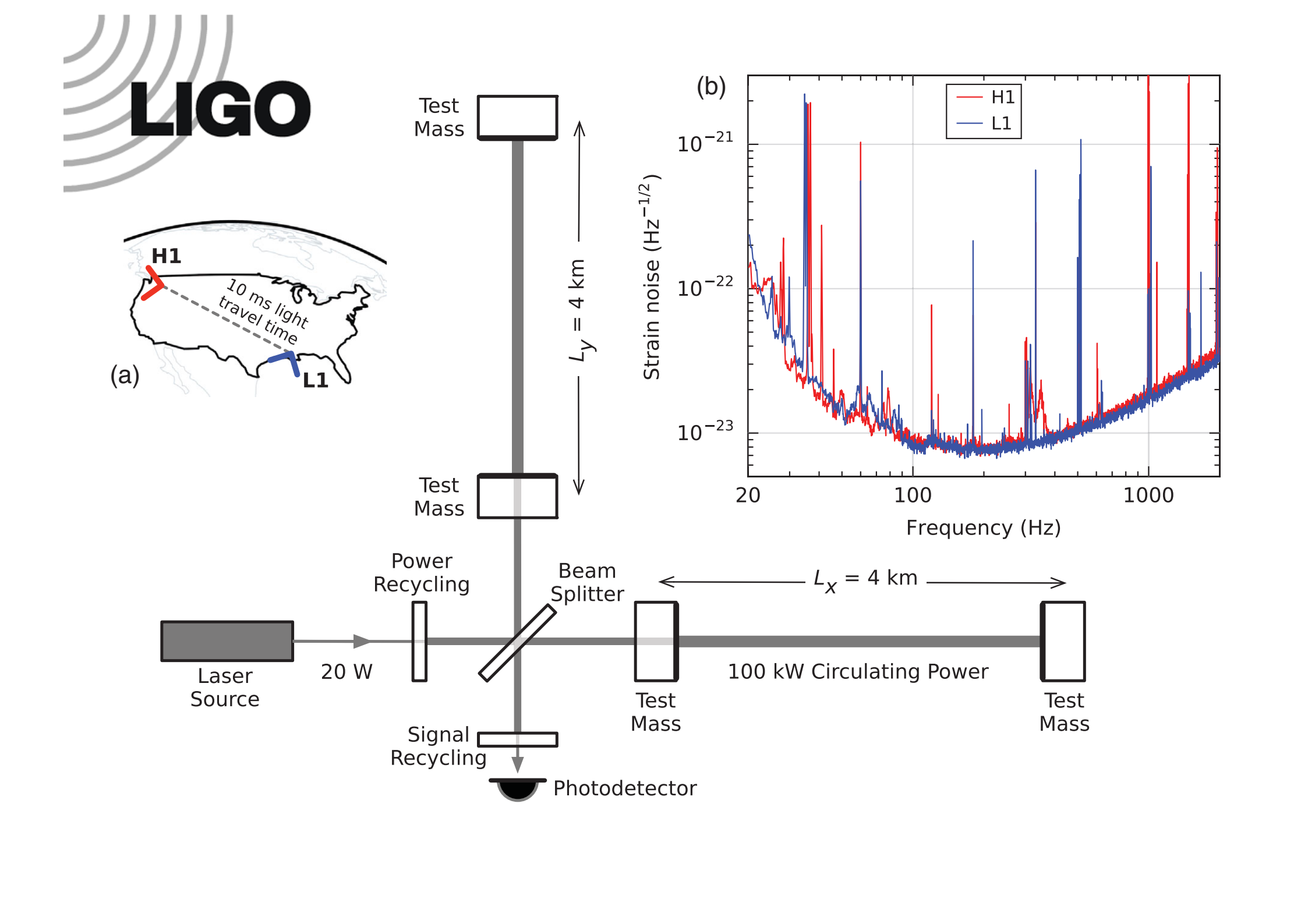
LIGO
(a)
H1
L1
10 ms light travel time
(b)
H1
L1
Strain noise (Hz$^{-1/2}$)
10^{-21}
10^{-22}
10^{-23}
20
100
1000
Frequency (Hz)
Test Mass
Test Mass
L_y = 4 km
Power Recycling
Beam Splitter
L_x = 4 km
Laser Source
20 W
100 kW Circulating Power
Test Mass
Test Mass
Signal Recycling
Photodetector

Detectors: the present (II)

The VIRGO detector (L= 3 km) near Pisa, Italy

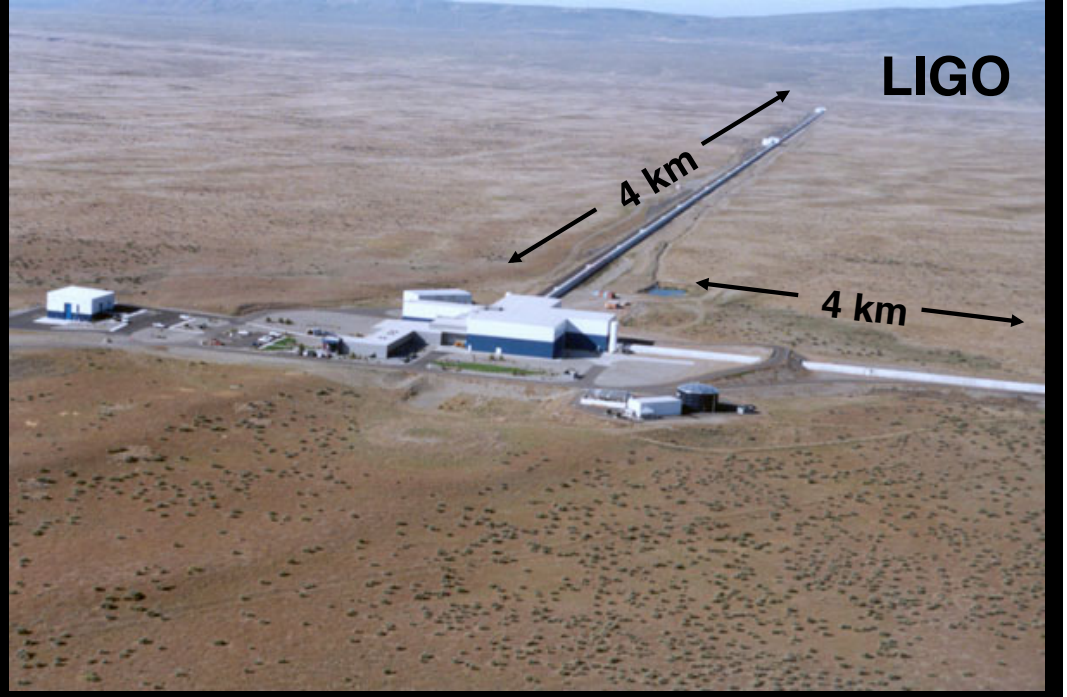
LIGO
4 km
4 km


VIRGO


LIGO


GEO 600

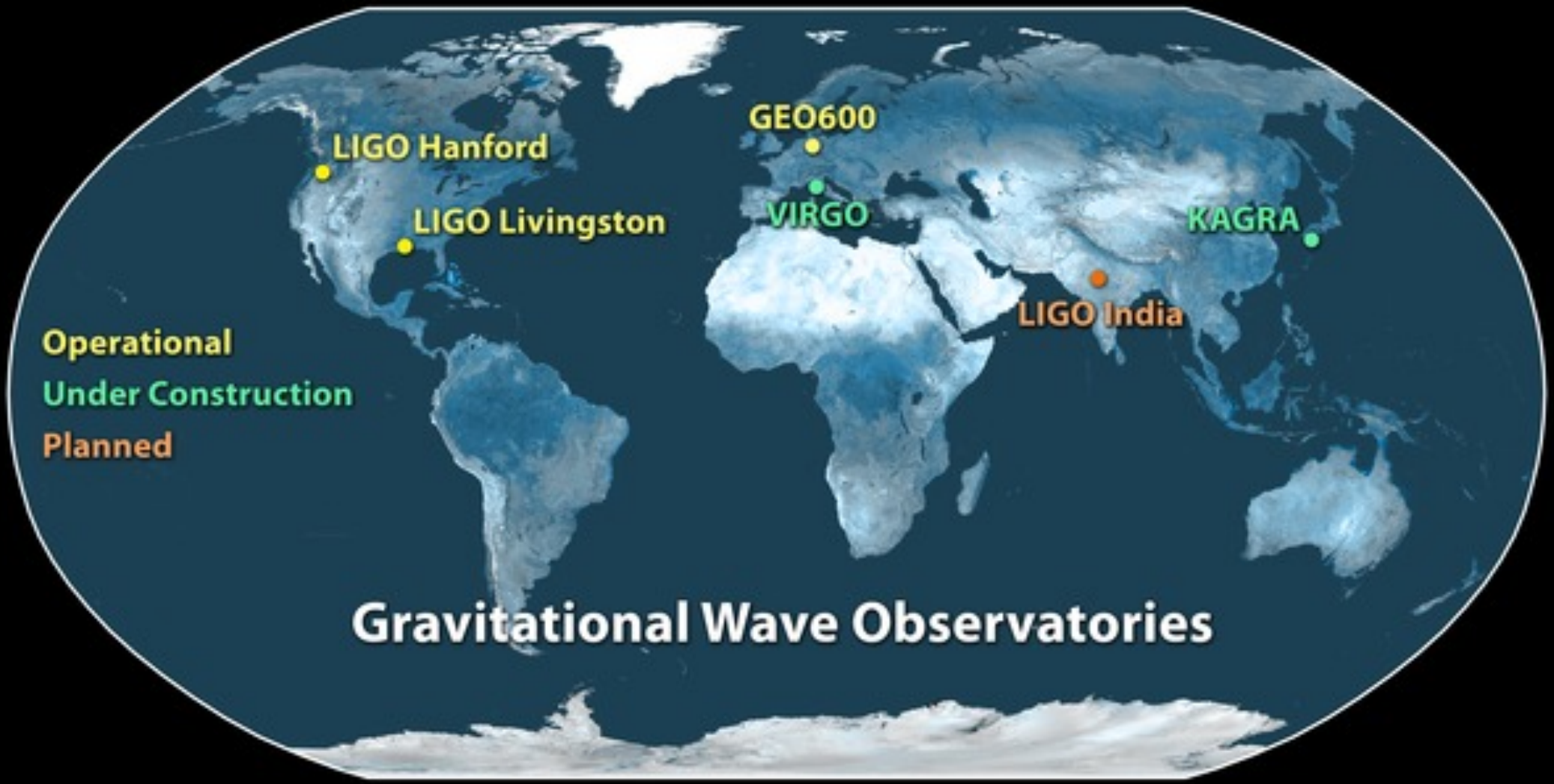
LIGO Hanford
GEO600
LIGO Livingston
VIRGO
KAGRA
LIGO India
Operational
Under Construction
Planned
Gravitational Wave Observatories

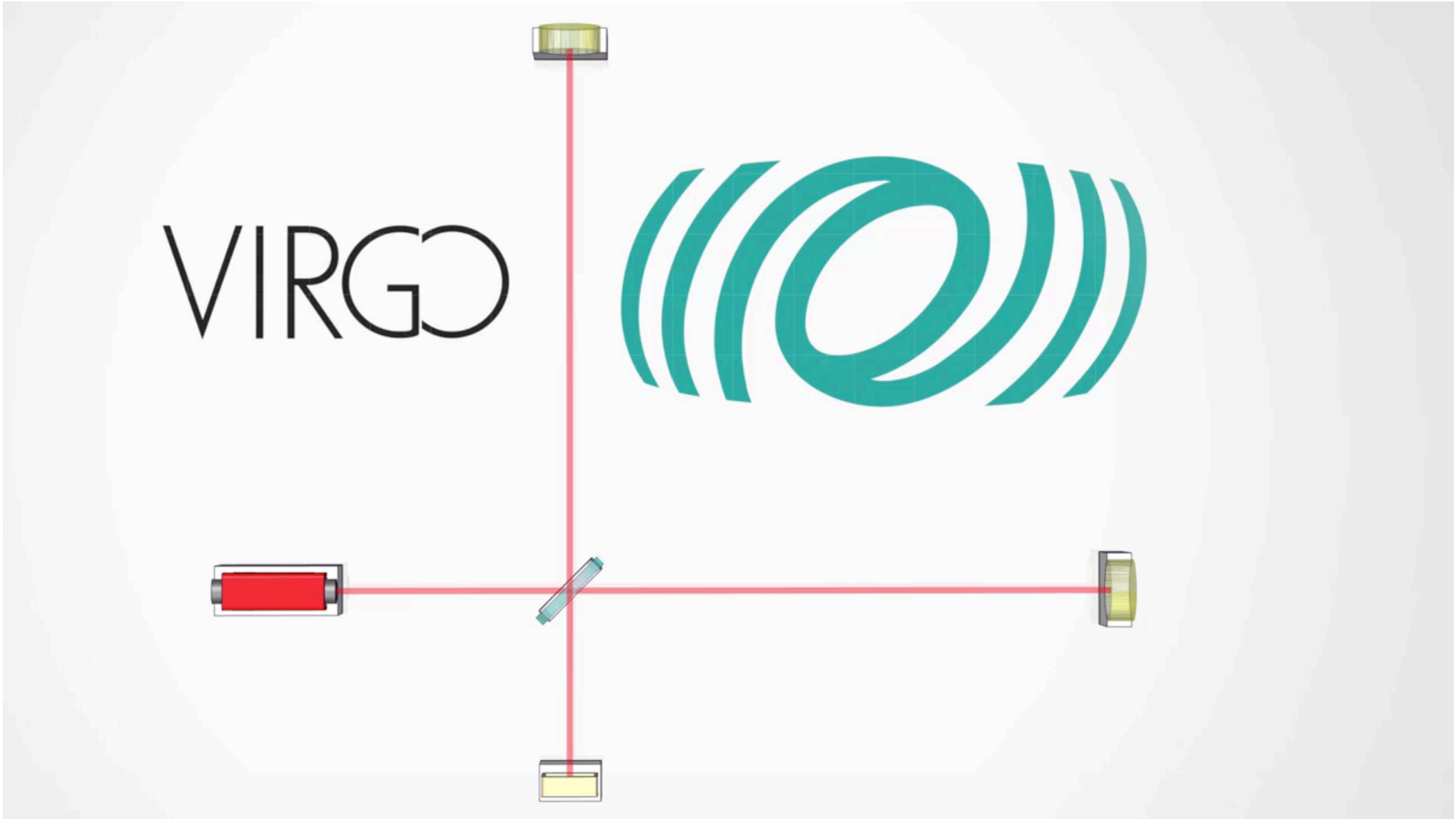
VIRGO

Going to space: the LISA detector

- Space-based detectors: “noise-free” environment, abundance of space!
- Long-arm baseline, low frequency sensitivity
- LISA: Up until recently a joint NASA/ESA mission, now an ESA mission only. To be launched around 2020.

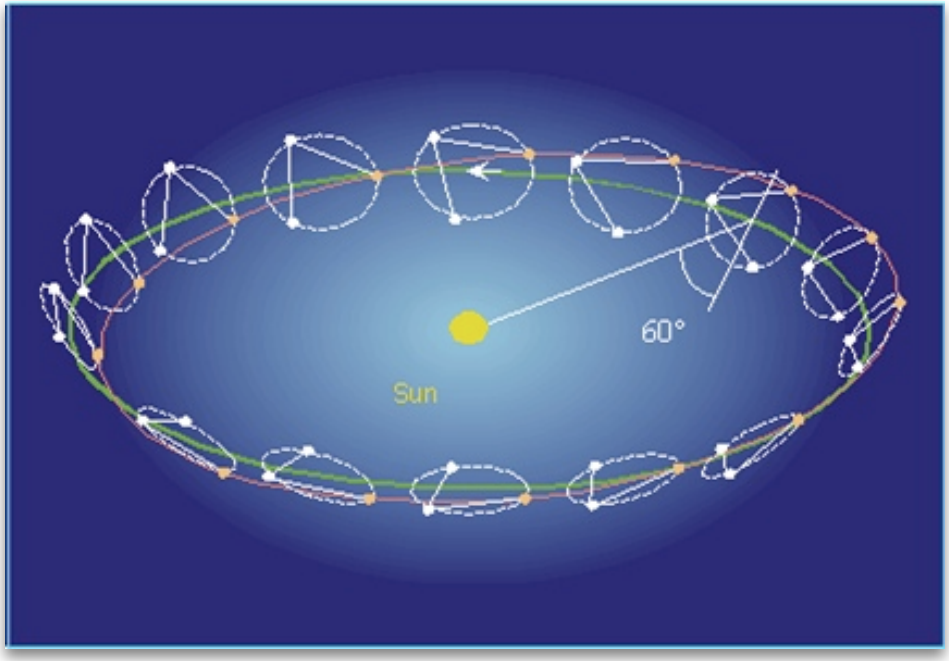

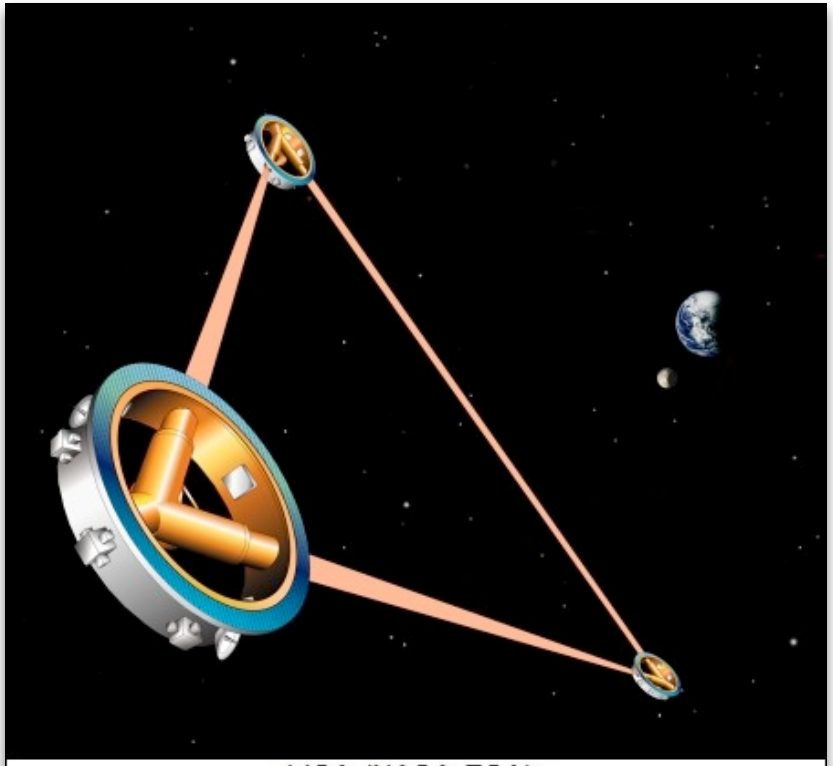
LISA (NASA-ESA)

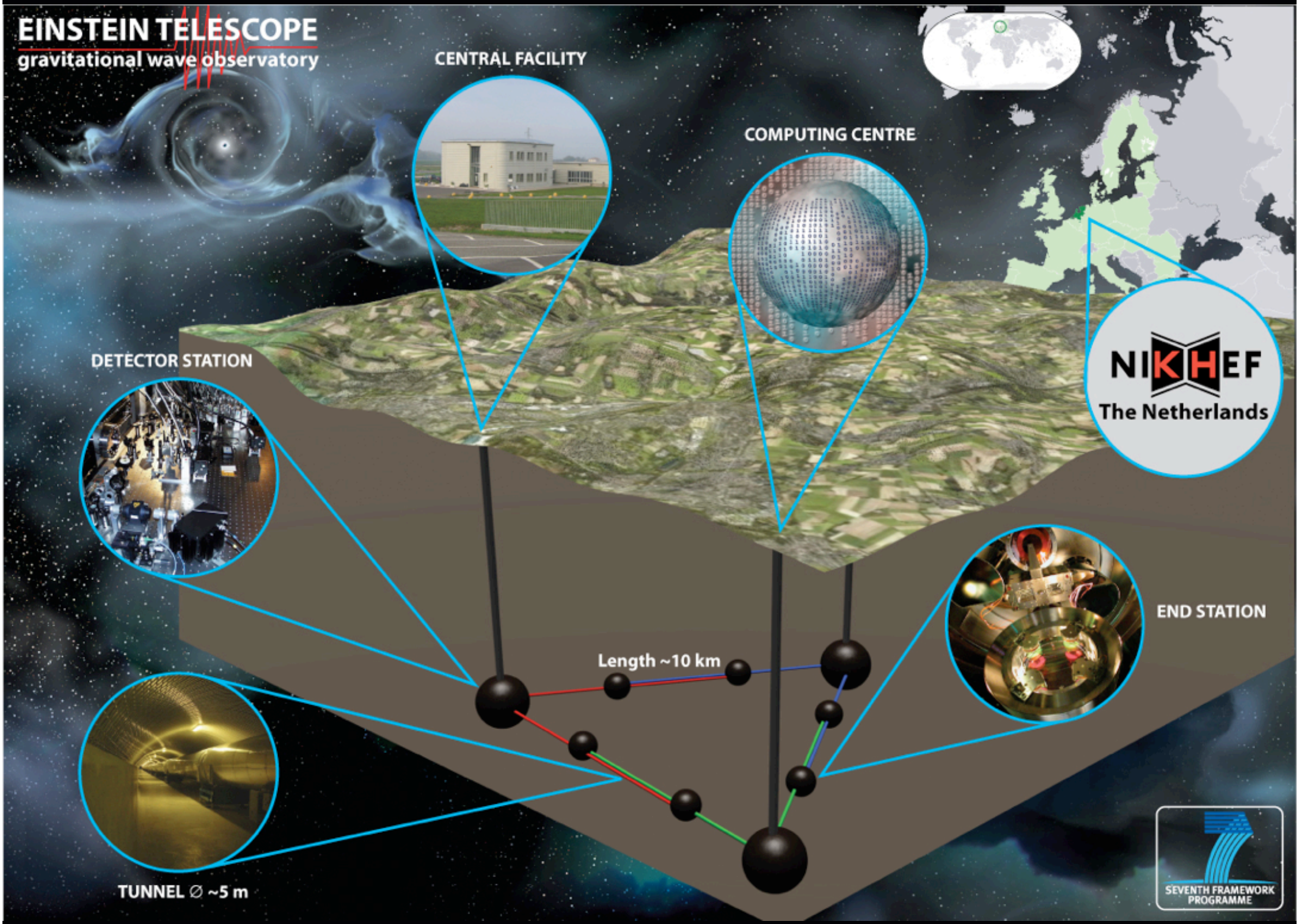
EINSTEIN TELESCOPE
gravitational wave observatory
CENTRAL FACILITY
COMPUTING CENTRE
NIKHEF
The Netherlands
DETECTOR STATION
END STATION
Length ~10 km
TUNNEL ∅ ~5 m
SEVENTH FRAMEWORK PROGRAMME

GWs detectors: ground and space

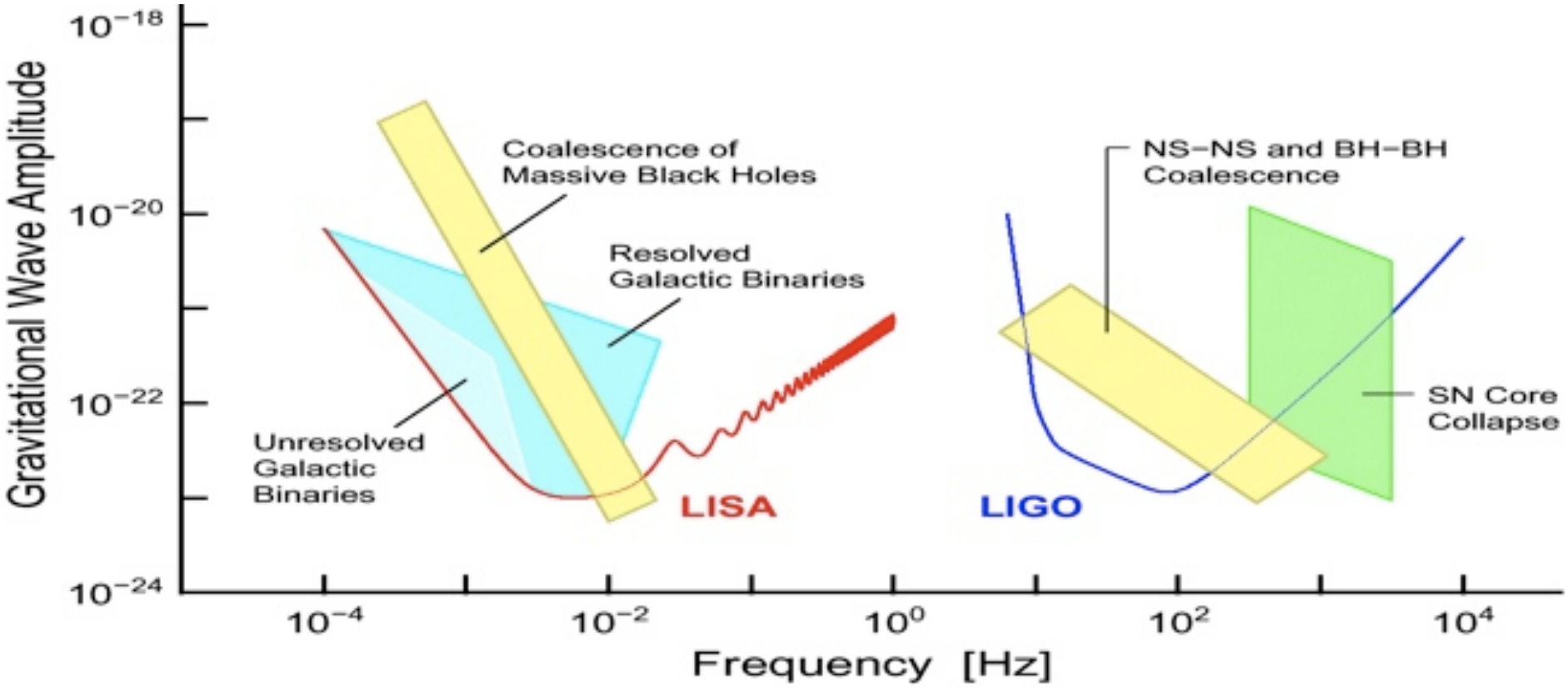

the discovery

PRL **116,** 061102 (2016)

Selected for a Viewpoint in *Physics*
PHYSICAL REVIEW LETTERS

week ending
12 FEBRUARY 2016

Observation of Gravitational Waves from a Binary Black Hole Merger

B. P. Abbott *et al.*[*]
(LIGO Scientific Collaboration and Virgo Collaboration)

(Received 21 January 2016; published 11 February 2016)

On September 14, 2015 at 09:50:45 UTC the two detectors of the Laser Interferometer Gravitational-Wave Observatory simultaneously observed a transient gravitational-wave signal. The signal sweeps upwards in frequency from 35 to 250 Hz with a peak gravitational-wave strain of 1.0×10^{-21}. It matches the waveform predicted by general relativity for the inspiral and merger of a pair of black holes and the ringdown of the resulting single black hole. The signal was observed with a matched-filter signal-to-noise ratio of 24 and a false alarm rate estimated to be less than 1 event per 203 000 years, equivalent to a significance greater than 5.1σ. The source lies at a luminosity distance of 410^{+160}_{-180} Mpc corresponding to a redshift $z = 0.09^{+0.03}_{-0.04}$. In the source frame, the initial black hole masses are $36^{+5}_{-4} M_{\odot}$ and $29^{+4}_{-4} M_{\odot}$, and the final black hole mass is $62^{+4}_{-4} M_{\odot}$, with $3.0^{+0.5}_{-0.5} M_{\odot} c^2$ radiated in gravitational waves. All uncertainties define 90% credible intervals. These observations demonstrate the existence of binary stellar-mass black hole systems. This is the first direct detection of gravitational waves and the first observation of a binary black hole merger.

DOI: 10.1103/PhysRevLett.116.061102

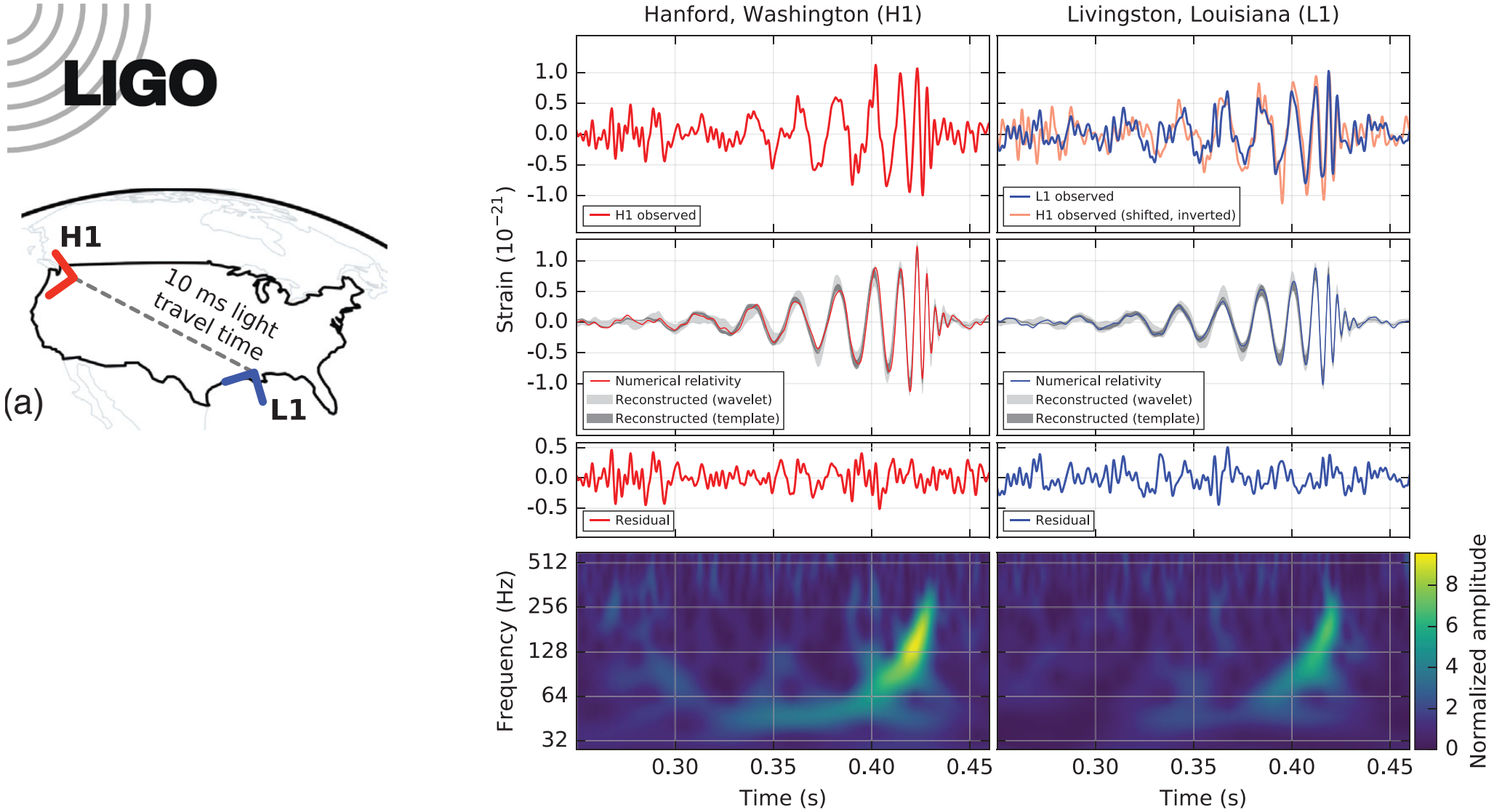

FIG. 1. The gravitational-wave event GW150914 observed by the LIGO Hanford (H1, left column panels) and Livingston (L1, right column panels) detectors. Times are shown relative to September 14, 2015 at 09:50:45 UTC. For visualization, all time series are filtered with a 35–350 Hz bandpass filter to suppress large fluctuations outside the detectors' most sensitive frequency band, and band-reject filters to remove the strong instrumental spectral lines seen in the Fig. 3 spectra. *Top row, left:* H1 strain. *Top row, right:* L1 strain. GW150914 arrived first at L1 and $6.9^{+0.5}_{-0.4}$ ms later at H1; for a visual comparison, the H1 data are also shown, shifted in time by this amount and inverted (to account for the detectors' relative orientations). *Second row:* Gravitational-wave strain projected onto each detector in the 35–350 Hz band. Solid lines show a numerical relativity waveform for a system with parameters consistent with those recovered from GW150914 [37,38] confirmed to 99.9% by an independent calculation based on [15]. Shaded areas show 90% credible regions for two independent waveform reconstructions. One (dark gray) models the signal using binary black hole template waveforms [39]. The other (light gray) does not use an astrophysical model, but instead calculates the strain signal as a linear combination of sine-Gaussian wavelets [40,41]. These reconstructions have a 94% overlap, as shown in [39]. *Third row:* Residuals after subtracting the filtered numerical relativity waveform from the filtered detector time series. *Bottom row:*A time-frequency representation [42] of the strain data, showing the signal frequency increasing over time.

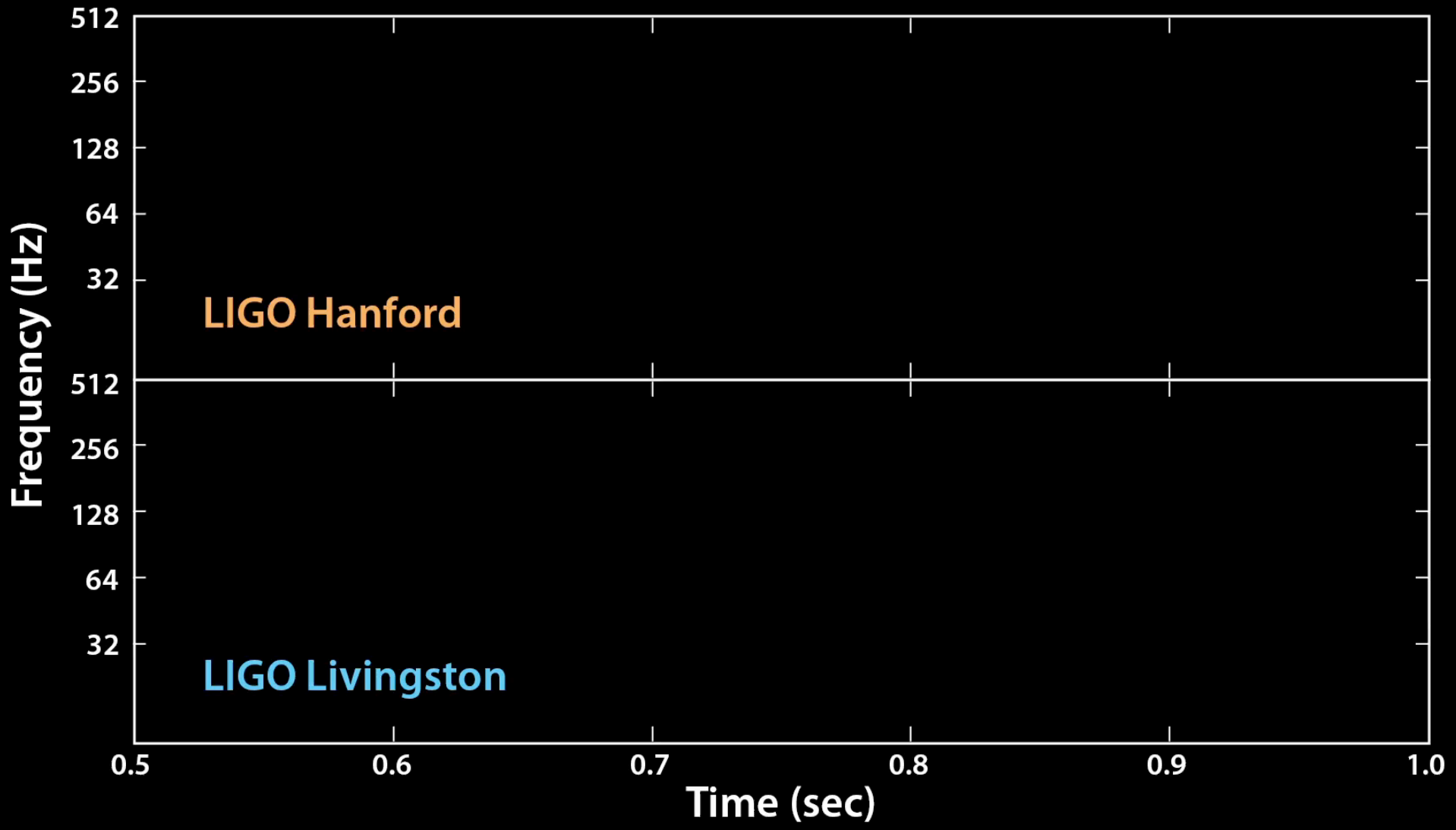
512
256
128
64
32
LIGO Hanford
512
256
128
64
32
LIGO Livingston
Frequency (Hz)
0.5
0.6
0.7
0.8
0.9
1.0
Time (sec)

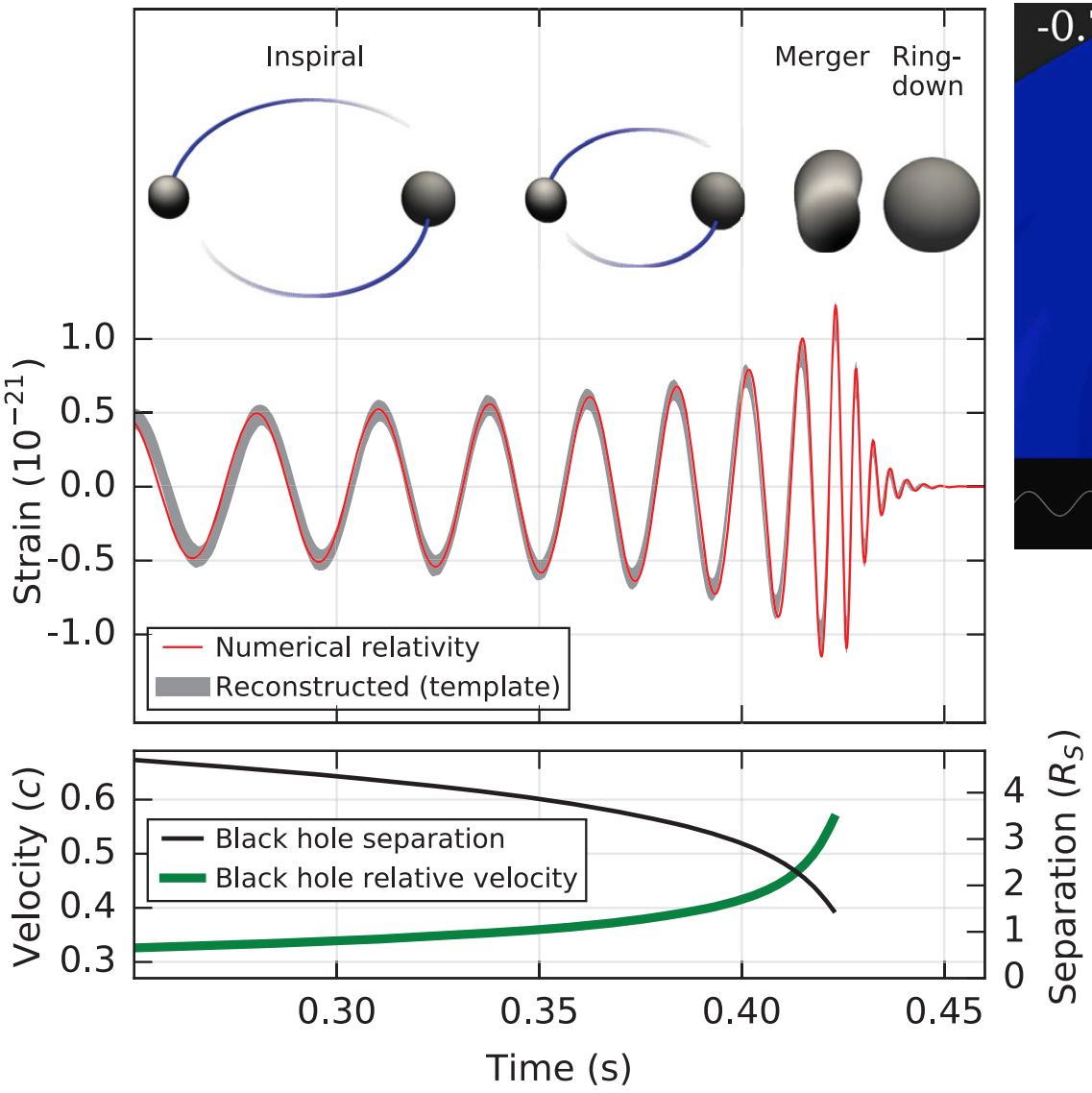

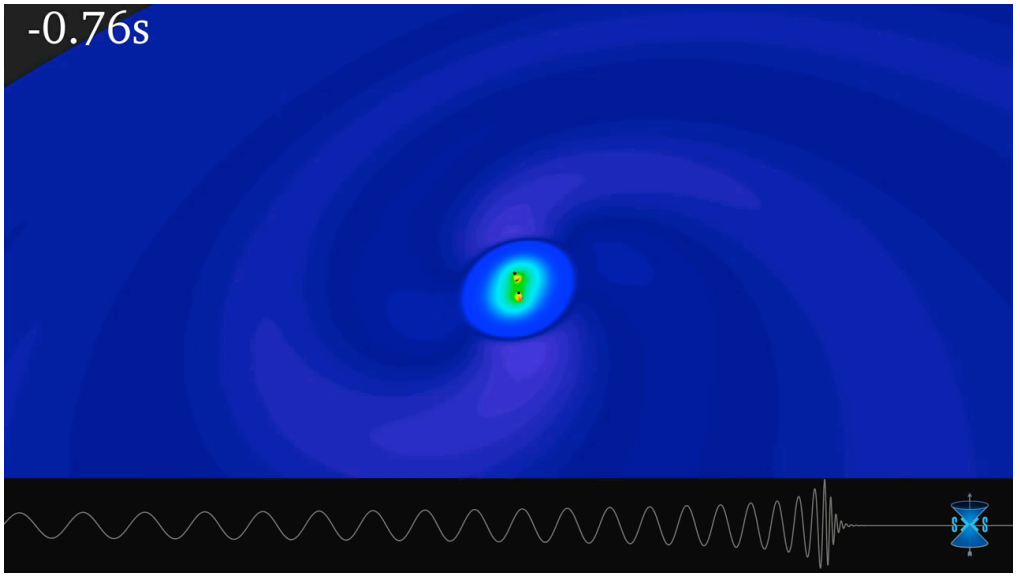

two black holes merge

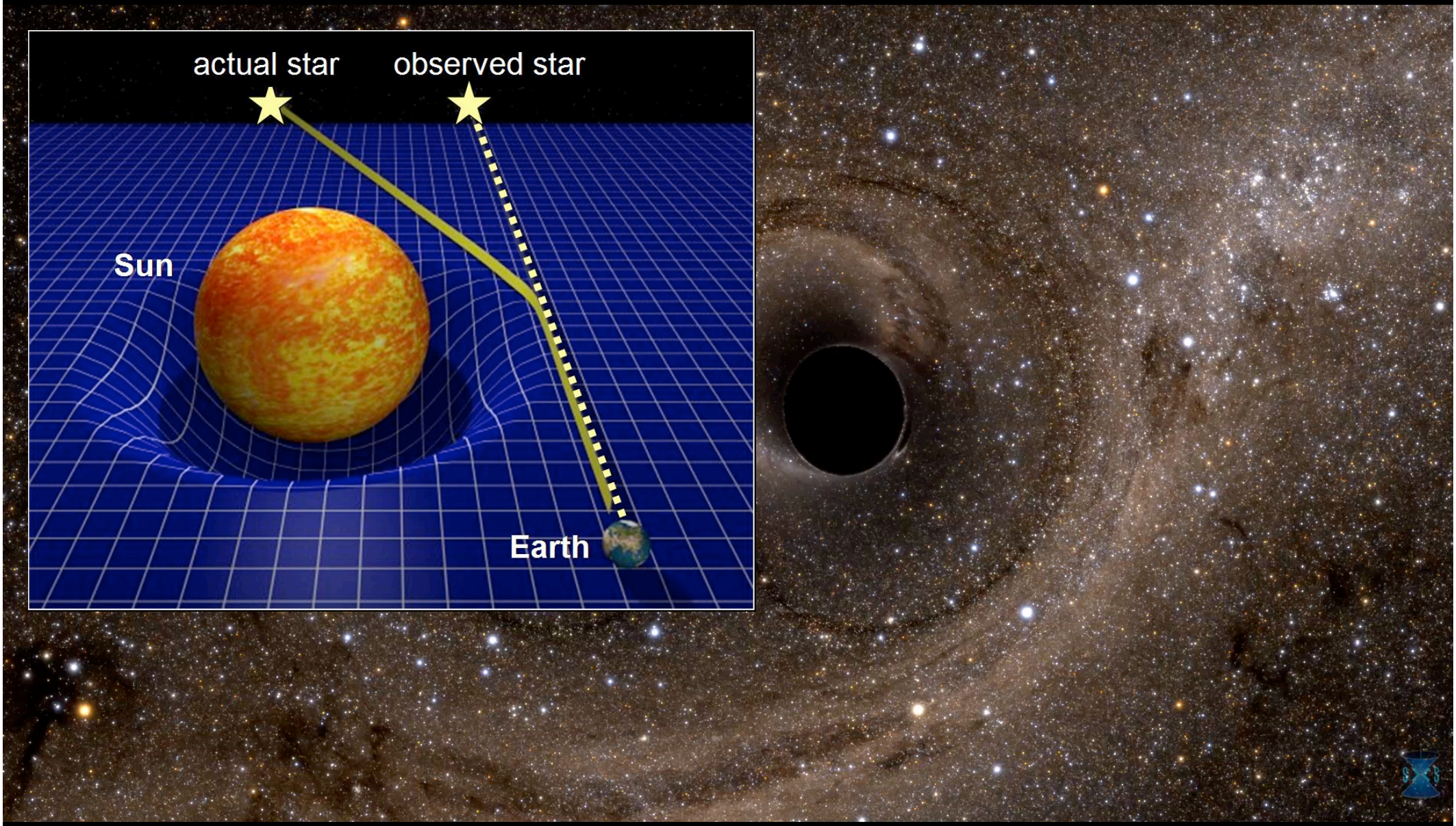
actual star
observed star
Sun
Earth

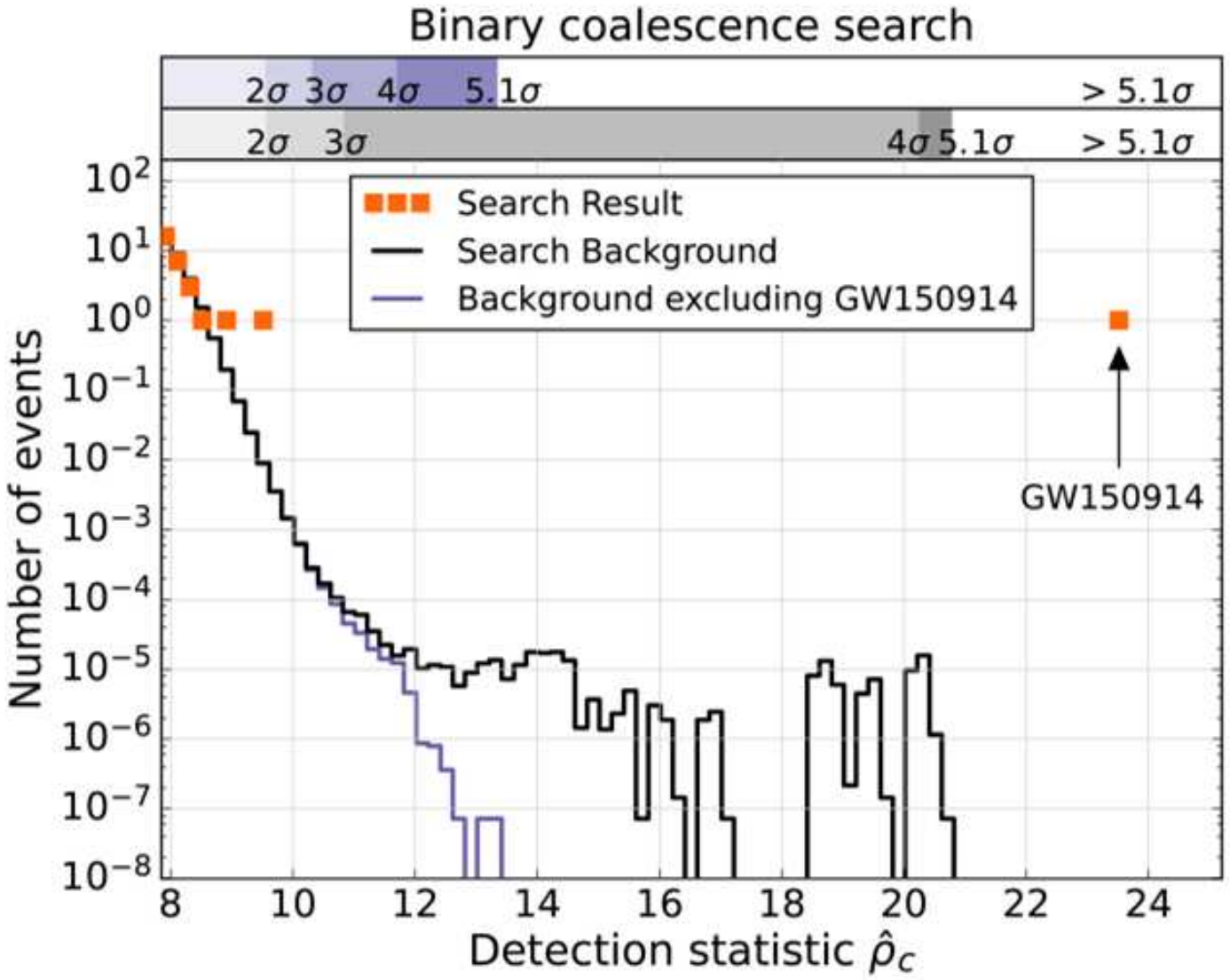

Figure 4. *(Adapted from figure 4 of our publication). Results from our binary coalescence search quantifying how rare GW150914 was compared with false 'events' resulting from noise fluctuations. This search concluded that a noise event mimicking GW150914 would be extremely rare – less than one occurrence in about 200,000 years of data like this – a value that corresponds to a detection significance of more than 5 'sigma'.*

location of GW source on sky

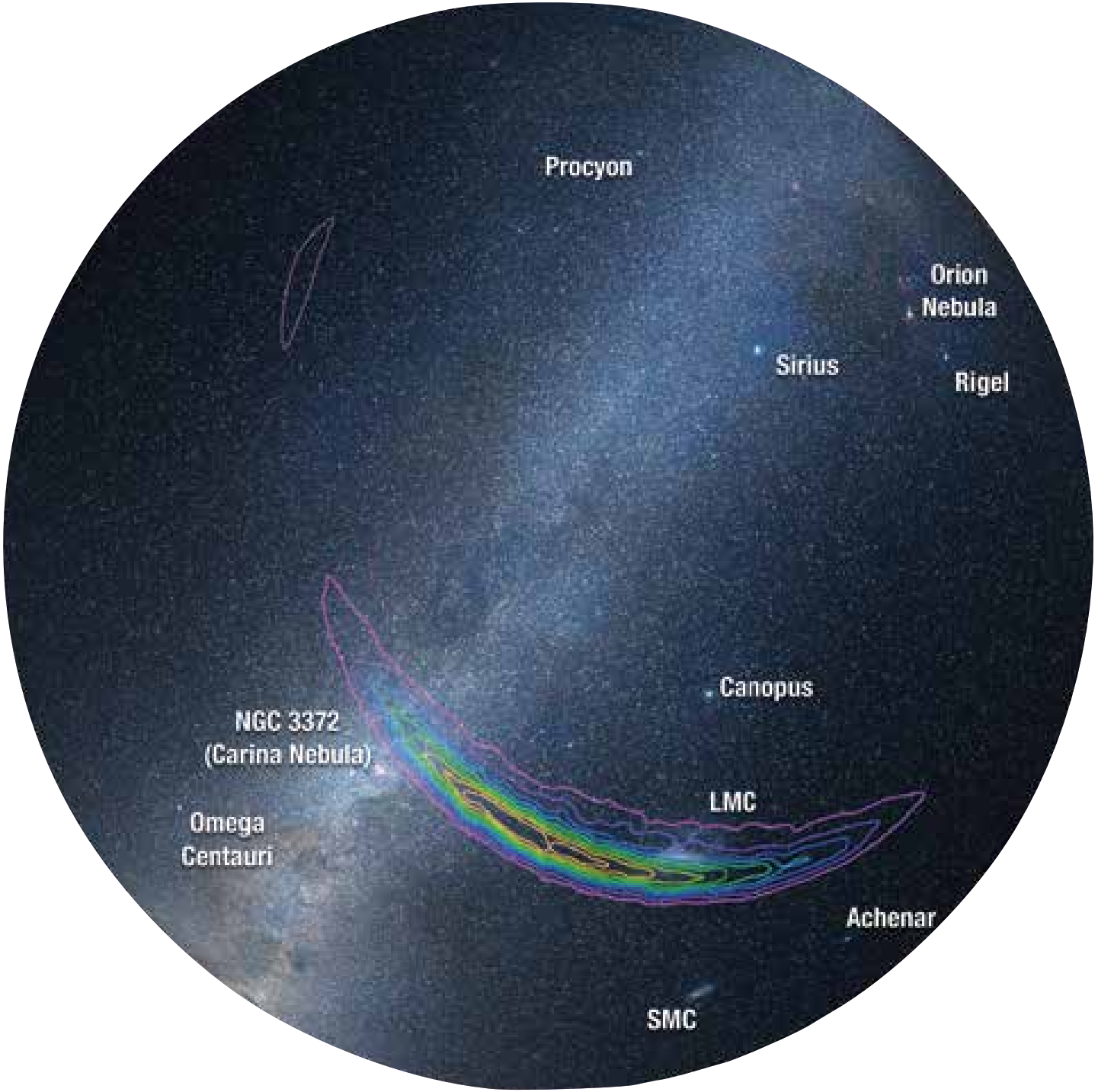

LIGO Scientific Collaboration

GW151226: OBSERVATION OF GRAVITATIONAL WAVES FROM A 22 SOLAR MASS BINARY BLACK HOLE COALESCENCE

A few months after the first detection of gravitational waves from the black hole merger event GW150914, the Laser Interferometer Gravitational-Wave Observatory (LIGO) has made another observation of gravitational waves from the collision and merger of a pair of black holes. This signal, called GW151226, arrived at the LIGO detectors on 26 December 2015 at 03:38:53 UTC.

The signal, v
a compact b
are one of
Gravitationa
system, caus
objects close
binary stretc
and squashi
information

GW151226 is
the LIGO Sci
marks the b
the frontiers

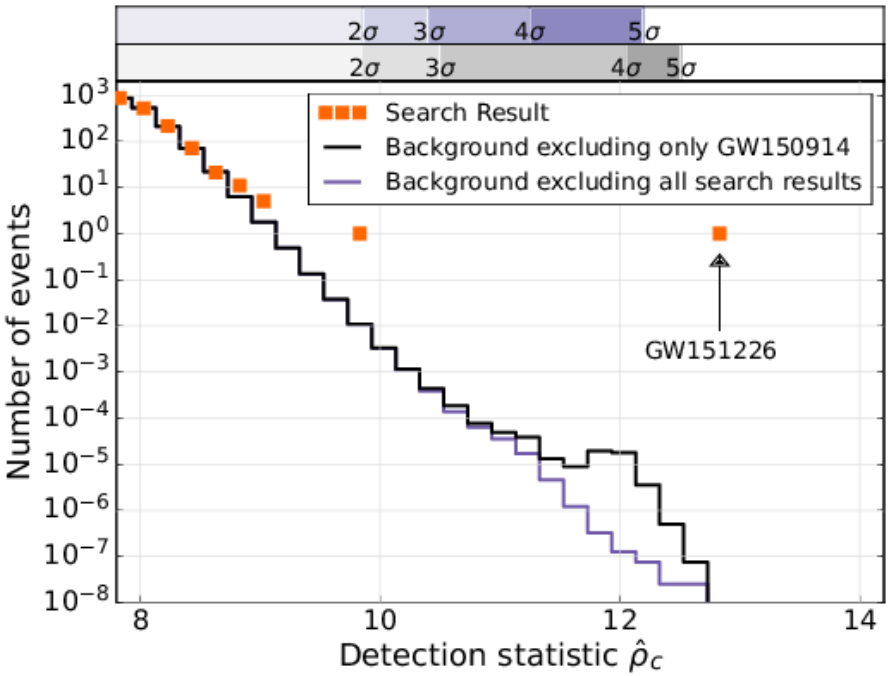

Figure 2: *(Adapted from figure 2 of our publication). Results from our search for gravitational wave sources similar to GW151226 (and the previous detection GW150914) showing the significance of this detection compared to a background of false 'events' caused by noise from the LIGO instruments. We see that GW151226 is detected well above the level of the background.*

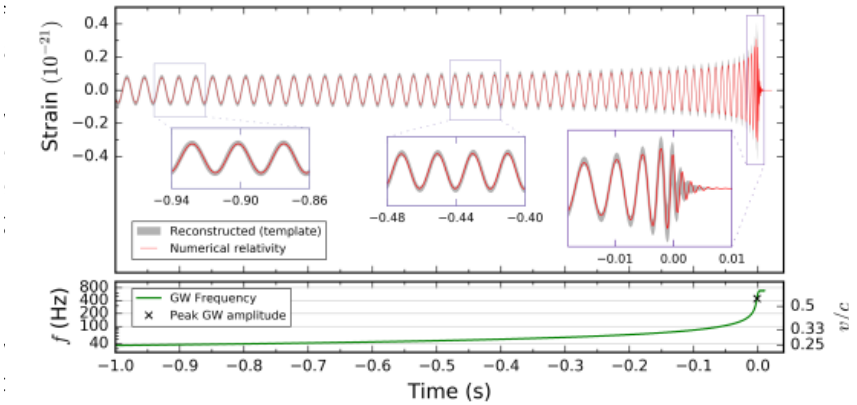

Figure 3: *(Adapted from figure 5 of our publication). The top panel shows a comparison of the reconstructed gravitational-wave strain signal over time as seen by the Livingston detector (gray) with a signal calculated from a numerical relativity simulation. The time is counting down in seconds leading up to the merger of the two black holes at zero. The lower panel shows how the frequency of the gravitational waves changes with time. The frequency increases as the black holes spiral together. This can also be related to the orbital velocity v, shown on the right hand side of the lower panel in units of the speed of light c. The black cross marks the point where the amplitude of the signal was largest, which is also approximately the time at which the black holes merged.*